Measuring the vertical response of the Galactic disc to an infalling satellite

Eloisa Poggio[1,2,★] Chervin F. P. Laporte[3,4,5,2], Kathryn V. Johnston[6,7], Elena D'Onghia[8], Ronald Drimmel[1] and Douglas Grion Filho[6]

[1] *Osservatorio Astrofisico di Torino, Istituto Nazionale di Astrofisica (INAF), I-10025 Pino Torinese, Italy*
[2] *Université Côte d'Azur, Observatoire de la Côte d'Azur, CNRS, Laboratoire Lagrange, France*
[3] *Institut de Ciències del Cosmos (ICCUB), Universitat de Barcelona (IEEC-UB), Martí i Franquès 1, 08028 Barcelona, Spain*
[4] *Kavli Institute for the Physics and Mathematics of the Universe (WPI), The University of Tokyo Institutes for Advanced Study (UTIAS), The University of Tokyo, Chiba 277-8583, Japan*
[5] *Department of Physics & Astronomy, University of Victoria, 3800 Finnerty Road, Victoria BC, V8P 5C2 Canada*
[6] *Department of Astronomy, Columbia University, 550 West 120th Street, New York, NY 10027, USA*
[7] *Center for Computational Astrophysics, Flatiron Institute, 162 5th Av., New York City, NY 10010, USA*
[8] *University of Wisconsin, Madison, Astronomy Department, 475 N Charter Str., Wisconsin, USA*

Accepted XXX. Received YYY; in original form ZZZ

ABSTRACT

Using N-body simulations of the Milky Way interacting with a satellite similar to the Sagittarius dwarf galaxy, we quantitatively analyse the vertical response of the Galactic disc to the satellite's repeated impacts. We approximate the vertical distortion of the Galactic disc as the sum of the first three Fourier azimuthal terms $m = 0$, 1 and 2, and observe their evolution in different dynamical regimes of interaction. After the first interaction, the $m = 0$ term manifests itself as outgoing ring-like vertical distortions. The $m = 1$ term (S-shape warp) is prograde when the impacts of the satellite are more frequent, or in general close to an interaction, whereas it is slowly retrograde in the most quiescent phases. The $m = 2$ term is typically prograde, and close to an interaction it couples with the $m = 1$ term. Finally, we find that the vertical response of the disc can be recovered in an unbiased way using the instantaneous positions and velocities of stars in a limited volume of the Galactic disc, analogous to real data, and that the measured vertical pattern speeds have a constraining power in the context of a Milky Way-satellite interaction.

Key words: Galaxy: disc – Galaxy: evolution – Galaxy: kinematics and dynamics – Galaxy: structure - galaxies: Local Group

1 INTRODUCTION

The Milky Way's vertical structure may hold important clues of its past formation. As soon as 21-cm surveys made it possible to study the distribution of neutral hydrogen gas around edge-on galaxies, it became apparent that many galaxies, including our own, are warped (Burke 1957; Kerr 1957). With the advent of large photometric surveys, such as the 2MASS and Sloan Digital Sky Survey, it became evident that the disc exhibited more complex behaviour in its vertical structure. In the solar neighbourhood, Widrow et al. (2012) uncovered signs of vertical waves in the form of North/South asymmetries in number density and bulk velocity of stars. The kinetic signatures of these waves were confirmed in Williams et al. (2013); Carlin et al. (2013); Schönrich & Dehnen (2018). Moreover, a growing number of observational studies suggested these waves could be part of much larger scale ones, giving rise to a warped and rippled disc (Xu et al. 2015; Price-Whelan et al. 2015; Li et al. 2017).

A number of mechanisms have been proposed to explain the existence/persistence of warps in galaxies. These have ranged from special configurations (and assumptions) such as the presence of flattened potential around discs (Sparke & Casertano 1988; Dubinski & Kuijken 1995), torques exerted by rotating halos (Nelson & Tremaine 1995), misaligned angular momenta between halo and disc (Debattista & Sellwood 1999) to misaligned gas infall (López-Corredoira et al. 2002) and the influence of external perturbers (Weinberg 1998), in particular through the excitation of global dark matter wakes which can penetrate deep into the Galactic midplane as well as tidal interactions. In particular satellite interactions are a prime mechanism to producing not only warps (e.g. Kim et al. 2014; Gómez et al. 2017; Semczuk et al. 2020), but also the more complex structure such as the generation of bending waves (e.g. Gómez et al. 2013; Widrow et al. 2014; D'Onghia et al. 2016), rings (Younger et al. 2008; Kazantzidis et al. 2009) and kinematic features as tidal tails (Toomre & Toomre 1972; D'Onghia et al.

★ E-mail: eloisa.poggio@inaf.it

2010; Laporte et al. 2019a) which are seen in the Milky Way (e.g. Grillmair 2006; Slater et al. 2014; Laporte et al. 2021). In fact, tidal encounters are central to the lifetime of galaxies in a cosmological context, as every central galaxy is surrounded by a subhalo population which can in some cases (depending on the mass and distance reached by a subhalo) shape the evolution of Galactic discs (e.g. Font et al. 2001; Gauthier et al. 2006; Aumer & White 2013; Giammaria et al. 2021). The thinness of the disc sets stringent limits on the infall rate of satellite systems, found to be no more than 4% of the total mass inside the Solar radius in our Galaxy (Toth & Ostriker 1992). Given the characteristic functional form of the subhalo mass function (Springel et al. 2008), the less numerous but much more dynamically impactful subhalos are the more massive ones.

In the Milky Way, potential suspects have long been the Magellanic Clouds (Weinberg & Blitz 2006) and the Sagittarius dwarf (Ibata & Razoumov 1998; Bailin 2003) galaxy (though with mixed success until more recently). While the Magellanic Clouds are more massive, they are also more distant, and new proper motion measurements (Kallivayalil et al. 2013) indicate that they are on a first infall, implying only a very recent interaction. However, first infall N-body models of the Large Magellanic Cloud (Laporte et al. 2018a) show that they are still able to warp the Galactic disc similarly to the HI observations (Levine et al. 2006) through the excitation of a wake which may be traced using the stellar halo (e.g. Garavito-Camargo et al. 2019). On the other hand, Sagittarius (hereafter, Sgr) is currently undergoing full disruption, and has been perturbing the Galaxy for a more extended period of time through numerous pericentric passages. Moreover, recent estimates of its total stellar progenitor mass place it at higher infall halo masses (e.g. Gibbons et al. 2017) which significantly raises its potential to shape the Galaxy. In particular, it has been proposed that Sgr could be an architect for spiral structure in the Milky Way (Purcell et al. 2011) and the formation of bending waves seen in the solar neighbourhood and at large distances (Gómez et al. 2013) at least in a qualitative sense. Recent N-body simulations of Sgr-like interactions with the Milky Way (Laporte et al. 2018b; Hunt et al. 2021) show that it is possible to simultaneously reproduce the amplitude of the density fluctuations in the solar neighbourhood and the extent of known outer disc structures (Newberg et al. 2002; Rocha-Pinto et al. 2004).

Thanks to the second *Gaia* Data Release (hereafter, *Gaia* DR2, Gaia Collaboration et al. 2018a), the complexity in kinematics and richness in terms of substructure of the Galactic disc has been mapped to greater detail and unprecedented spatial coverage around the Sun (Gaia Collaboration et al. 2018b). Vertical disturbances, streaming motions, wave patterns and arches in the velocity space have been revealed on a large scale (Ramos et al. 2018; Poggio et al. 2018; Romero-Gómez et al. 2019; Friske & Schönrich 2019), triggering new interest and questions into the physical mechanisms regulating the dynamical evolution of the disc (Carrillo et al. 2019; López-Corredoira et al. 2020; Poggio et al. 2020). Complementary to the earlier findings of Widrow et al. (2012), when viewed in 2D, the vertical phase-space distributions of stars in the solar neighbourhood revealed spiral snail-shell features (Antoja et al. 2018), signaling that the disc is out of equilibrium and currently undergoing phase-mixing, possibly caused by Sgr (Laporte et al. 2018b; Antoja et al. 2018; Binney & Schönrich 2018; Laporte et al. 2019b; Haines et al. 2019; Bland-Hawthorn et al. 2019; Bland-Hawthorn & Tepper-Garcia 2020). Alternatively, phase-space spirals have been suggested as a manifestation of internal mechanisms, such as the bar buckling instability (Khoperskov et al. 2019). However, a density decomposition as a function of stellar ages of the phase-spiral might suggest this is not the origin in the Milky Way (see Laporte et al. 2019b). The sharper view of Gaia DR1 combined with the SDSS's long baseline to provide accurate proper motions, and later those of *Gaia* DR2, has also revealed remnants and confirmed earlier signs of ancient massive accretion events, among which stands out the Gaia Enceladus-Sausage galaxy (Meza et al. 2005; Navarro et al. 2011; Belokurov et al. 2018; Helmi et al. 2018; Haywood et al. 2018; Recio-Blanco 2018; Helmi 2020), thought to have occurred about 10 Gyr ago.

With the increasing complexity faced by the data and the number of competing dynamical processes which could occur in concert, it is now imperative to study and develop theoretical models to help with the interpretation of observations. Ultimately, one would want to discriminate between the different dynamical processes that might be at play (bar buckling, misaligned gas accretion, halo rotation, satellite(s) interaction(s)...). Recently, the vertical response of galactic discs to multiple external perturbers has been revisited in some detail by Chequers et al. (2018), who compared the behaviour of bending waves in the presence of a population of dark matter subhalos and in isolation. However, the tidal effects are dominated by the most massive and luminous substructures, and many subhalos never reach the central part of a halo (Font et al. 2001). Thus, a complementary approach to Chequers et al. (2018) is to study the response of a Galactic disc subject to a minor merger over a lifespan of several orbital timescales on a polar orbit. This should help get a better intuition of the effect of a particular kind of orbital configuration shared by at least one massive known luminous satellite of the MW, the currently disrupting Sgr dwarf.

In this work we aim to explore the reaction of a Milky Way-like disc to a massive Sgr-like satellite as it spirals deeper into the galactic potential. The forthcoming Gaia Data Release 3 and other future datasets will afford even more detailed and global views of the Galaxy, motivating us to perform a Fourier analysis of the disc vertical distortion, which may be feasible with stellar data. In this paper, we aim to: (i) characterize the response of the disc to the repeated impacts of the dwarf galaxy, (ii) study the connection between the satellite's orbit and the disc response; (iii) investigate whether the response might be reliably measured from a limited data volume; (iv) understand whether the vertical response of the disc has a constraining power in the context of a Milky Way-Sgr-like interaction. In a companion work, we look at the influences that drive this evolution (Grion Filho et al. 2020).

The paper is structured as follows. In Section 2, we describe the simulations used in this study. In Section 3, we define and discuss different dynamical regimes present in the MW-Sgr interaction process. Section 4 is dedicated to the analysis of the disc vertical response to the repeated interactions with the Sgr-like satellite. In Section 5, we compare the actual evolution of the disc obtained in Section 4 to the results that would be obtained from a volume-limited survey. Finally, we summarise and discuss our our results in Section 6.

2 SIMULATIONS

The simulations analysed here are taken from the pre-Gaia DR2 runs performed in Laporte et al. (2018b) (hereafter L18). These consist of a series of controlled N-body experiments aimed at studying the response of a MW-like system to Sgr and LMC-like perturbers. Despite its modest setup, this simulation was used to establish that the large scale perturbations in the outer disc such as the Monoceros Ring complex (Newberg et al. 2002;

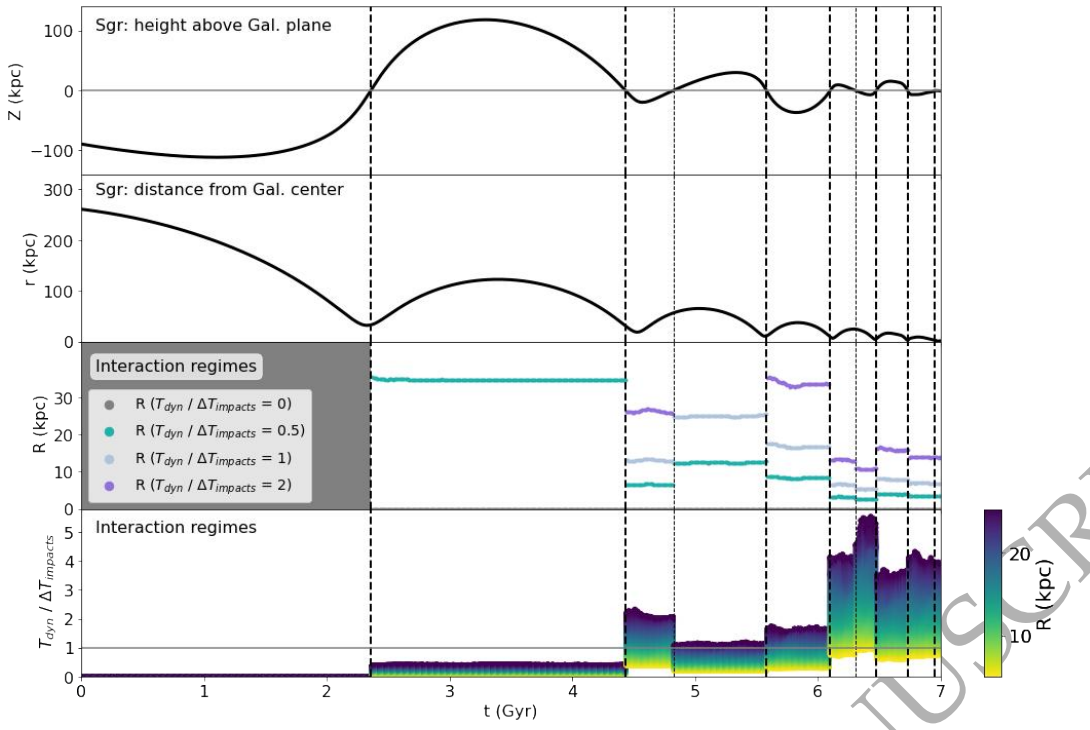

Figure 1. *From top to bottom: First panel*: Vertical elevation of Sgr with respect to the Galactic plane as a function of time, based on Sgr L2 model. *Second panel*: Same as before, but showing the distance of Sgr from the Galactic center. *Third panel*: The temporal evolution of the Galactocentric radius R in the Galactic disc corresponding to four fixed time-scale ratios $T_{\rm dyn}/\Delta T_{\rm impacts}$ = 0, 0.5, 1, 2, which are associated to four different dynamical regimes of interaction between Sgr and the Milky Way (see Section 3). The corresponding radius R=R($T_{\rm dyn}/\Delta T_{\rm impacts}$) is calculated by taking the average azimuthal velocity $\langle V_\phi \rangle$ at a given time. *Fourth panel*: The range of radii (shown by the colour-coding) where the ratio $T_{\rm dyn}/\Delta T_{\rm impacts}$ reaches a given value, indicating different regimes of interation. The grey horizontal line shows where $T_{\rm dyn}/\Delta T_{\rm impacts}$ = 1, which roughly corresponds Regime 2. In all three panels, the dashed vertical lines indicate Sgr's plane-crossings (i.e. where Z=0). Due to a different response of the disc (see text), we have made a distinction between the plane-crossings in proximity (thick dashed vertical lines) and distant from (thin dashed vertical lines) Sgr's nearest pericenter.

Slater et al. 2014; Deason et al. 2018), TriAnd (Rocha-Pinto et al. 2004) and small scale inner disc perturbations (Widrow et al. 2012; Antoja et al. 2018) can be simultaneously understood as the response of the Galactic disc to perturbations from a satellite like Sgr (Laporte et al. 2018b, 2019a). A number of observaitonal studies had suggested a disc interpretation for outer stellar halo-disc interface structures (Price-Whelan et al. 2015; Xu et al. 2015; Li et al. 2017; de Boer et al. 2018; Sheffield et al. 2018) and were later confirmed through chemistry (e.g. Bergemann et al. 2018; Hayes et al. 2018). It was also the first N-body simulation used to interpret the Gaia DR2 RVS velocity fields and phase-space spiral in Gaia DR2 and study its formation with a realistic model of a Sgr-like satellite interaction (Laporte et al. 2019b). The simulations were also used to predict the formation of structures like the Anticenter stream (Laporte et al. 2019a) as remnants of tidal arms excited by satellite interaction and the expected modulation of the star formation history of the Galaxy following the impacts which was first reported in (Laporte et al. 2020) using the outer disc Monoceros complex and recently in the solar neighbourhood (Ruiz-Lara et al. 2020).

In this paper, we take a closer look at the L2 run, which considered the interaction between a MW-like host and a Sgr-like progenitor with $M_{SGR200} = 6 \times 10^{10}\,{\rm M}_\odot$ infalling from the virial radius. For more details on the simulations and their analysis, we refer the reader to L18, but provide a brief summary here to guide the discussion. For all runs, a fiducial host Milky Way-like model was adopted consisting of a disc of $M_d = 6.5{\times}10^{10}\,{\rm M}_\odot$ in mass, with an exponential profile in the radial direction and isothermal vertically with scale radius $R_d = 3.5\,$kpc and scale height $z_d = 0.53\,$kpc, a Hernquist bulge with $M_b = 10^{10}\,{\rm M}_\odot$ and scale length $a_b = 0.7\,$kpc surrounded by a dark matter halo of mass $M_{200} = 10^{12}\,{\rm M}_\odot$ approximated by a Hernquist (1990) profile with scale length $a_h = 53\,$kpc which is adiabatically contracted according to the prescription of Blumenthal et al. (1986). This results in a galaxy with a rotation curve consistent with McMillan (2011). The disc particles have mass $m_d = 1.0 \times 10^4\,{\rm M}_\odot$ while dark matter halo particles have mass $m_{dm} = 2.6 \times 10^4\,{\rm M}_\odot$. The initial conditions were realised with GalIC (Yurin & Springel 2014) and the galaxy was set with a Toomre $Q > 1.5$ to avoid the formation of non-axisymmetric features in the isolated case. This choice is arbitrary of course and only intended for the sake of the numerical experiment at the time to understand the response of the disc in the absence of internal perturbations from the start. For comparison, a run with the same initial conditions but without Sgr is presented in Appendix C .

Throughout the paper, we analyse the disc's dynamics in the simulation from a reference frame centered around the Galactic Center with respect to the Galactic midplane. This is achieved using the same analysis methods outlined in Gómez et al. (2013); Laporte et al. (2018b), which involve centering the galaxy through the iterative shrinking sphere algorithm (Power et al. 2003) and realigning the system with respect to the total angular momentum of the inner disc. As a result, any re-orientation or precession of the disc w.r.t. to its initial configuration resulting from interactions (e.g. Velazquez & White 1999; Gómez et al. 2017) will be lost. This dynamical response is not studied in this paper.

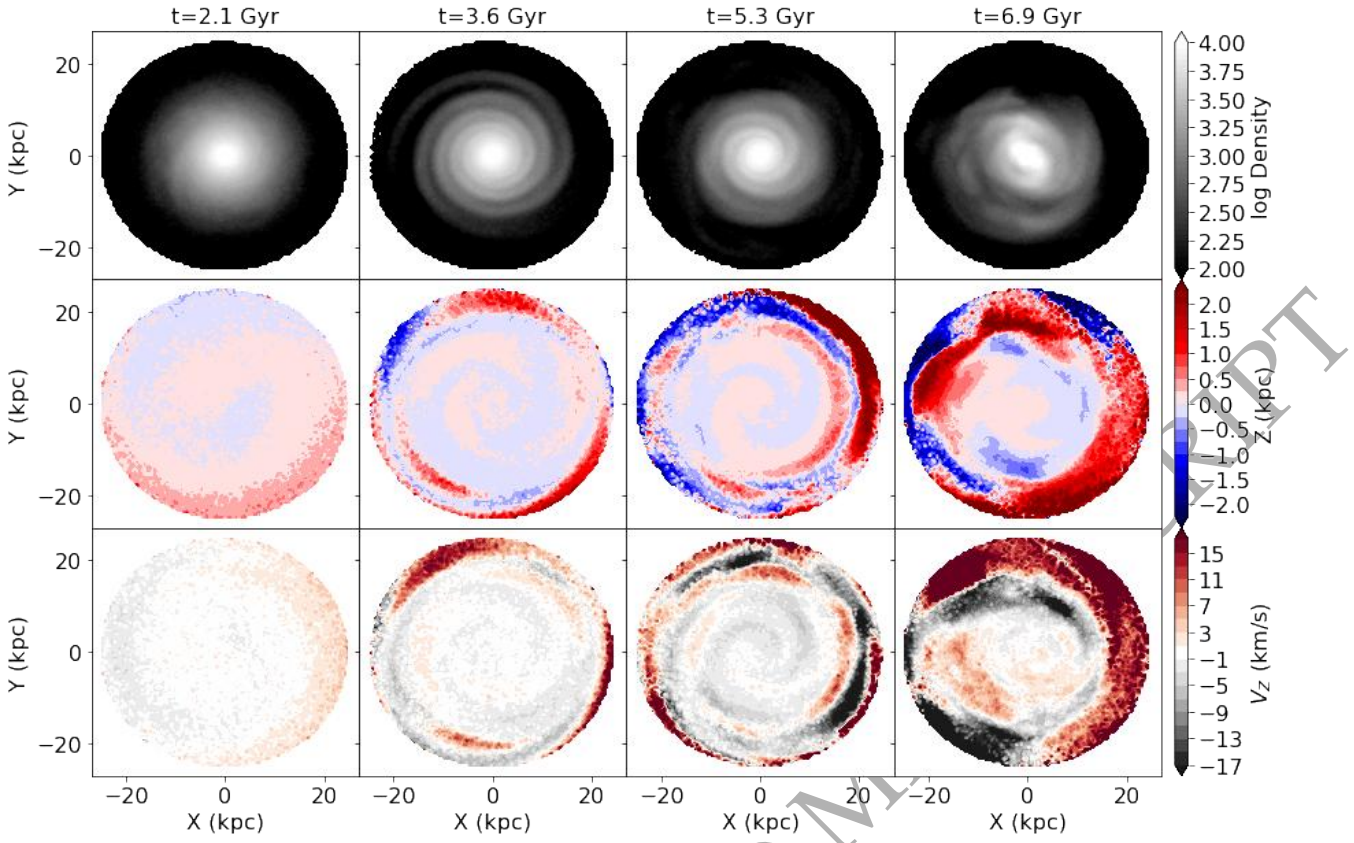

Figure 2. Face-on views of the Milky Way's disc in the four interaction regimes (see text): surface density (upper row), mean vertical coordinate Z (middle row) and vertical velocity Vz (lower row) at different times. At t=2.1 Gyr (first column) no impacts with Sgr have occured. At t=3.6 Gyr (second column), t=5.3 Gyr (third column), t=6.9 Gyr (fourth column), the galactic disc has experienced, respectively, one, three and eight impacts. Disc rotation is clockwise.

3 INTERACTION REGIMES

The interaction process between Sgr and the Galactic disc can be divided into different regimes, based on the the orbit of Sgr and the dynamical properties of the disc.

At time t=0, the progenitor of Sgr is launched into orbit and crosses the Galactic plane several times before merging fully with the Milky Way. As time passes, plane-crossings become more frequent (Figure 1, top panel), with Sgr passing through the Galactic plane (z=0 kpc) at 2.36, 4.43, 4.83, 5.58, 6.1, 6.31, 6.48, 6.73 and 6.95 Gyr (dashed vertical lines in Figure 1). At the plane-crossings, Sgr is located at 32, 30, 55, 11, 9, 24, 5, 2.5 and 1 kpc from the Galactic center, respectively. As can be seen in Figure 1, most (but not all) of the plane-crossings are close to the orbit pericenters.

As discussed in the following section, the influence of Sgr becomes progressively more important as its orbit gets closer to the MW and the impacts become more frequent. However, the response to Sgr is not the same everywhere in the Galactic disc. We define the dynamical time $T_{\rm dyn}$ (i.e. Galactic year) as a function of Galactocentric radius R, i.e. $T_{\rm dyn} \sim 2\pi R/V_\phi$, where V_ϕ is the mean azimuthal velocity. For example, for stars rotating at $V_\phi \sim 230$ km/s, the dynamical time would be $\sim$ 220 Myr at R = 8 kpc, or $\sim$ 550 Myr at R = 20 kpc.

We define different Sgr-MW interaction regimes based on the ratio $T_{\rm dyn}/\Delta T_{\rm impacts}$, where $T_{\rm dyn}$ is the above-defined dynamical time of the disc, and $\Delta T_{\rm impacts}$ is the time interval between two impacts of Sgr. As shown in Figure 1 (bottom), the ratio $T_{\rm dyn}/\Delta T_{\rm impacts}$ demarcates four different regimes:

- **Regime 0** or pre-interaction regime: $T_{\rm dyn}/\Delta T_{\rm impacts} \sim 0$, as $\Delta T_{\rm impacts} \sim \infty$. The disc effectively evolves in isolation.
- **Regime 1**: $0 < T_{\rm dyn}/\Delta T_{\rm impacts} < 1$. In this Regime, interaction time-scales are long enough to give the disc the possibility to relax between one and the other plane-crossing (although long-live modes induced by Sgr's passage can survive.)
- **Regime 2**: $T_{\rm dyn}/\Delta T_{\rm impacts} \sim 1$. Since the disc dynamical time is of the same order of the time interval between two impacts, the disc doesn't have time to fully relax after an interaction.
- **Regime 3**: $T_{\rm dyn}/\Delta T_{\rm impacts} > 1$. This is the most perturbed regime, where the repeated impacts on short time-scales in the inner disc cause a strong and complicated response in the Galactic disc.

As shown in Figure 1 (third and fourth panel), the interaction regime strongly depends on radius R. As a result, for a given time, different regimes may coexist at different radii.

While this simulation is not an exact reconstruction of the MW-Sgr interaction, it is useful to consider what point in the simulation is most similar to the present-day Milky Way-Sgr system. Based on current data (Ibata et al. 1994; Johnston et al. 2005; Law & Majewski 2010; Peñarrubia et al. 2010), Sgr's position in the Milky Way is just below the Galactic plane, at about $\sim$ 16 kpc

from the Galactic center. Considering the L2 model, the most similar geometry is at the 4th and 5th plane-crossings (i.e. R$\sim$ 10 kpc), which occurs between Regime 2 and 3.

4 VERTICAL RESPONSE OF THE DISC

4.1 Qualitative overview

Here, we qualitatively discuss the response of the disc to the repeated impacts of Sgr. Although it is not the main objective of this paper, it is instructive to observe the evolution of the disc stellar density (Figure 2, first row). The disc is initially smooth (first panel), and develops a grand design spiral structure after the first interaction (second panel). After three disc crossings, spiral arms are not as well-defined as before, and present small-scale discontinuities in the outer parts (third panel). Finally, after eight disc crossings, the spiral arms are disrupted and a central bar is formed (fourth panel).

Different interaction regimes clearly manifest themselves also in the vertical dimension (Figure 2, second row). The disc initially exhibit a mild S-shape warp (first panel), just before the first disc crossing. After the first interaction with Sgr, the distortion of the disc remains relatively smooth, but spiral waves are excited (second panel, see following Sections for a deeper analysis). Such waves can be clearly seen for R < 15 kpc, are trailing, but do not spatially coincide with the spiral arms observed in the density. As plane crossings become more frequent and Sgr gets closer to the disc, the vertical distortion becomes more prominent (third panel), until vertical features loose their coherence over large portions of the Galactic disc (fourth panel).

A similar behaviour is observed in the mean vertical motions V_Z (Figure 2, third row), which appear to be related to the vertical distortion in Z (see Figure 2, second row, and later discussion on the connection between Z and V_Z).

A qualitative impression from Figure 2 already gives a taste of the response of the disc to different interaction regimes, but a quantitative analysis is needed to understand the physical mechanisms governing the evolution of the disc under the repeated interactions with a satellite. In the following Sections, we will concentrate on the vertical dimension, quantitatively analyze its temporal evolution and discuss its connection with Sgr's orbit.

4.2 Fourier analysis of vertical oscillations

In this Section, we quantify the vertical response of the disc by means of a Fourier analysis. For a given ring at Galactocentric radius R, we express the mean Z as a sum of infinite Fourier terms terms in Galactic azimuth ϕ:

$$Z(R,\phi) = A_0(R) + \sum_{m=1}^{\infty} A_m(R)\cos(m\phi - \Phi_m(R)) \quad , \tag{1}$$

where $A_0(R)$ is the amplitude of the Fourier term $m = 0$ at a given R, which is a constant with respect to ϕ, while $A_m(R)$ and $\Phi_m(R)$ are, respectively, the amplitude and phase of the vertical terms $m \geq 1$. The azimuthal angle ϕ is taken as positive in the direction of Galactic rotation. Rings in R are created in such a way that they contain the same number of particles (40 000), implying that they are more concentrated in the inner regions, and less dense in the disc outskirts. This causes the most external ring to be at $\simeq$ 23 kpc, beyond which the requested number of particles cannot be reached.

In this paper, we follow the method used by Chequers et al. (2018); Chequers & Widrow (2017) to study m=1 bending waves in an isolated Milky Way-like disc and under the continuous bombardment of sub-halos. However, our approach is somewhat complementary to their analysis, as we analyse the response of the disc to a single massive Srg-like perturber, with the specific goal of identifying typical behaviours in different dynamical regimes of interaction.

Figure 3 illustrates the power of Fourier decomposition. For a given radius R, every term m can be summarized by either one (for $m = 0$) or two (for $m \geq 1$) numbers, indicating, respectively, the amplitude, or amplitude and phase. This makes the approach particularly convenient, because we can reduce to some extent the degree of complexity observed in the disc vertical response (first column) by applying a Fourier decomposition, and analyzing the temporal evolution of the amplitudes and phases of the single terms separately (second, third and fourth column). As will become apparent in the following, this approach allows us to identify several features, which otherwise would have been buried within the complexity of the disc response.

For practical reasons, we first aim to understand whether some Fourier terms are more relevant than others, so that we can devote our attention to the dominant ones, and observe their evolution over time. Figure 4 shows which Fourier vertical term is dominant at a given time and a given distance from the Galactic center. Vertical dashed lines show Sgr's plane crossings. The plot summarises in a compact manner the evolution of the disc: a vertical slice corresponds to a single snapshot of the simulation, while a horizontal slice shows the temporal evolution at a given annulus at R in the Galactic disc. We can clearly see that the most relevant terms are $m = 0, 1$ and 2. In contrast, the mode $m = 3$ makes a minor contribution, and higher terms are completely absent. Based on the above considerations, in the rest of the paper we will focus on the first three terms, $m = 0, 1$ and 2.

4.2.1 *Overview of the responses in different regimes*

The separate evolution of the $m = 0, 1$ and 2 amplitudes is shown in Figure 5. As we can see, in general, interactions with Sgr are typically associated with a significant increase in the amplitude, for all three terms. Then, the amplitude oscillates a few times, with fluctuations that are more significant and longer lasting in the outer parts of the disc than in the inner regions. After that, the amplitudes of the three terms tend to go back to a semi-quiescent phase. However, before the second passage, the $m = 2$ term (bottom panel) exhibits a much higher amplitude than it had before the first one. This indicates that, while the time-scales in Regime 1 are expected to be long enough for the disc to relax, long-lived modes induced by Sgr's first passage continue to be present in the disc.

In the last part of the simulation, the dynamical time-scales of the satellite's orbit are not long enough for the outer disc to recover from each interaction. This effects manifests itself as a rapid increase after one interaction, followed by the above-mentioned oscillatory behaviour, but with a typically very short (Regime 2) or event absent (Regime 3) quiescent phase before another impact occurs.

It is also worth noting that not all plane-crossings have the same impact on the disc's behaviour. For example, during the plane-crossings at $\approx$ 4.9 and 6.1 Gyr, Sgr is far from pericenter (Figure 1), and the disc reaction is less relevant (or even irrelevant) compared to the other cases.

Finally, we note that the repeated impacts of Sgr on the Galactic disc cause a general amplitude increase of the Fourier vertical terms m=0,1 and 2 throughout the simulation, implying typically stronger

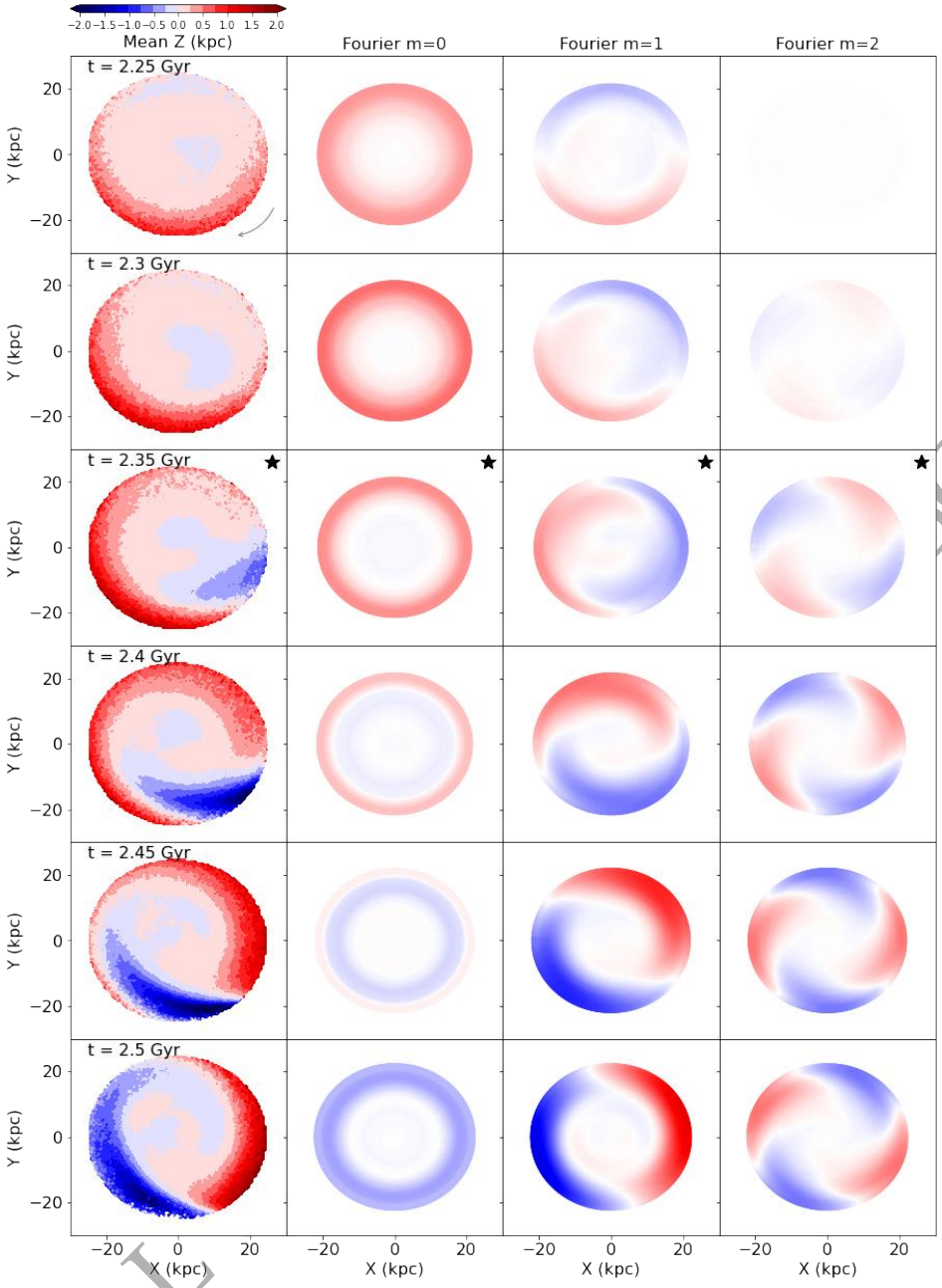

Figure 3. Face-on view of the mean vertical distortion of the Galactic disc during the first interaction with Sgr (first column), accompanied by the corresponding Fourier decomposition into the $m = 0$ (second column), $m = 1$ (third column) and $m = 2$ (fourth column) terms. The Galaxy rotates clockwise. The snapshot at t=2.35 Gyr has been marked by a black star, to highlight that an interaction with Sgr is taking place (the pericenter and plane-crossing occur, respectively, at 2.33 and 2.36 Gyr). The Fourier decomposition shows that: (i) Sgr excites ring-like vertical distortions (second column), which propagate from the inner to the outer parts of the disc; (ii) The $m = 1$ distortion moves in a prograde direction with respect to Galactic rotation; (iii) The $m = 2$ term is excited by the interaction with Sgr. An animated version of this figure is available for the entire simulation.

vertical distortions in the more perturbed regimes (Regime 2 and 3) than in the quiescent phases.

4.2.2 *Fourier vertical term m=0*

Unlike the other Fourier terms (where $A_m(R) > 0$ by definition), the amplitude of $m = 0$ can be either positive or negative. Figure 6 repeats the top panel of Figure 5, but this time color-coded by sign. In the outer parts of the disc, oscillations are clearly visible.

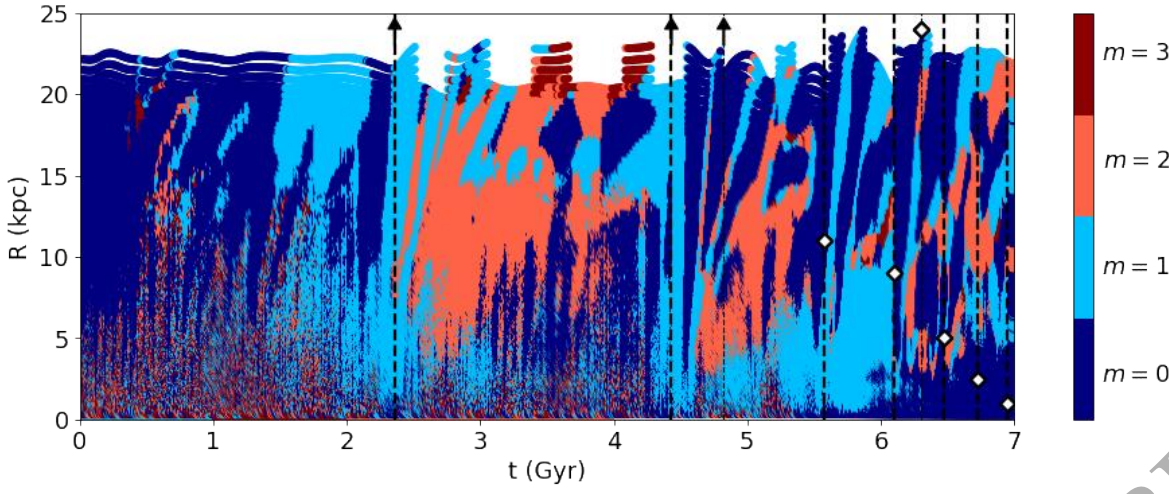

Figure 4. For a given time t and Galactocentric radius R, the Fourier term with the largest amplitude based on our analysis. Dashed vertical lines indicate plane-crossings of Sgr. The position of Sgr during a plane-crossing is indicated by a white diamond if $R_{\rm Sgr} < 25$ kpc. Otherwise, a black arrow is drawn at the top of the figure.

Late regimes (Regime 2 and 3) exhibit amplitudes up to 2 order of magnitudes larger than the early ones (Regime 0 and 1).

In response to an interaction, the $m = 0$ term manifests itself as a series of ring-like vertical perturbation of opposite sign, typically propagating from the inner to the outer disc, similar to a stone causing ripples to propagate out in all directions across the surface of a pond. Ring-like vertical distortions are propagating faster close to an interaction, and become much slower or almost static in quiescent phases. If the sign of A_0 is constant for all radii and the amplitude increases with R (e.g. vertical monochromatic features at ≈ 4.6 Gyr or 5.7 Gyr), the $m = 0$ mode forms an U-shaped bending mode (e.g. Reshetnikov & Combes 1998). This can happen in quiescent phases or in the immediate proximity of an interaction (before evolving into the above-mentioned outgoing vertical perturbations).

A visual representation of the $m = 0$ temporal evolution can be found in Figure 3, A2 and A3.

4.2.3 *Fourier vertical term m=1*

The m=1 term corresponds to a classical S-shape warp (e.g. Chen et al. 2019; Skowron et al. 2019) and might be the dominant Fourier term in the Milky Way (Levine et al. 2006). Following the approach of Chequers et al. (2018), Figure 7 shows the the temporal evolution of the m=1 phase angle. Such a plot can be used to determine the morphology of m=1 bending waves in the disc. Provided that the Galactic azimuth $\phi > 0$ is positive in the direction of Galactic rotation, one can dissect the plot horizontally, and observe the variation of the phase angle for a fixed radius R as a function of time. Hence, one can deduce if the phase angle (i.e. line-of-nodes of the warp) is moving in a prograde (towards $\phi > 0$) or retrograde (towards $\phi < 0$) direction with respect to Galactic rotation. Alternatively, one can dissect the plot vertically, and determine whether the line-of-nodes of the warp is straight (i.e. constant with R), leading (i.e. ϕ increases with increasing radius R) or trailing (i.e. ϕ decreases with increasing radius R).

After an initial relaxation time due to the non-equilibrium initial conditions, a clear coherent pattern manifests itself between $t \approx 0.9$ and ≈ 2.1 Gyr. At $R \approx 15$ kpc, the phase angle progressively changes from ≈ -45 deg (dark blue color) to -170 deg (light blue). A similar behaviour is observed at all Galactic radii, but especially in the outer parts, with the phase angle slowly moving towards $\phi < 0$, thus opposite to Galactic rotation. Moreover, for a given time, we can take a vertical slice of the plot, and observe that the phase angle varies towards $\phi > 0$ for increasing Galactic radii R, forming a leading spiral. For example, at $t \approx 2$ Gyr the phase angle is $\approx -180, -140$ and -100 deg, respectively, at $\approx 12, 16$ and 20 kpc. It is worth noting that this pattern is characterized by a long time-scale, which causes the line-of-nodes to vary slowly, with a period much larger than 1 Gyr.

A similar behaviour has been extensively discussed in several other works. Shen & Sellwood (2006) studied the evolution of an initially relaxed disc subjected to the torque of a massive outer torus, introduced to mimic the effect of a misaligned outer DM halo. The resulting torque caused the disc to precess in a retrograde direction, with an angular rate proportional to the distance from the Galactic center. Furthermore, the misalignment between the outer and the inner parts of the disc caused an additional torque, whose magnitude was comparable to the previous one. The geometry of the line-of-nodes (i.e. whether it was leading or trailing spiral pattern) indicated which one of the two torques was dominant. In isolation (i.e. without the torque from the torus), Shen & Sellwood (2006) found that the precession rate associated with the inner discâĂŹs torque generated a warp line-of-nodes with a leading spiral pattern. Gómez et al. (2016) studied a Milky Way-like galaxy in a cosmological hydrodynamical simulation, and explored the interaction between a satellite, the host halo, and the disc. They found that that the external source of the torque (i.e. the satellite causing a wake in the DM halo), which was responsible for the onset of the perturbation, decayed over time, leaving behind a misaligned outer disc. Then, the $m = 1$ line-of-nodes wrapped up into a leading spiral, indicating that the torque induced by the inner disc started to dominate right after the pattern was excited.

A pattern similar to the ones discussed above (i.e. slow retrograde precession, leading spiral geometry of the line-of-nodes) is found for the pre-interaction regime in this simulation, indicating that the self-gravity of the inner disc is dominant. For comparison, we also run a control-simulation with an isolated disc (i.e. without Sgr), finding a similar pattern (see Appendix C).

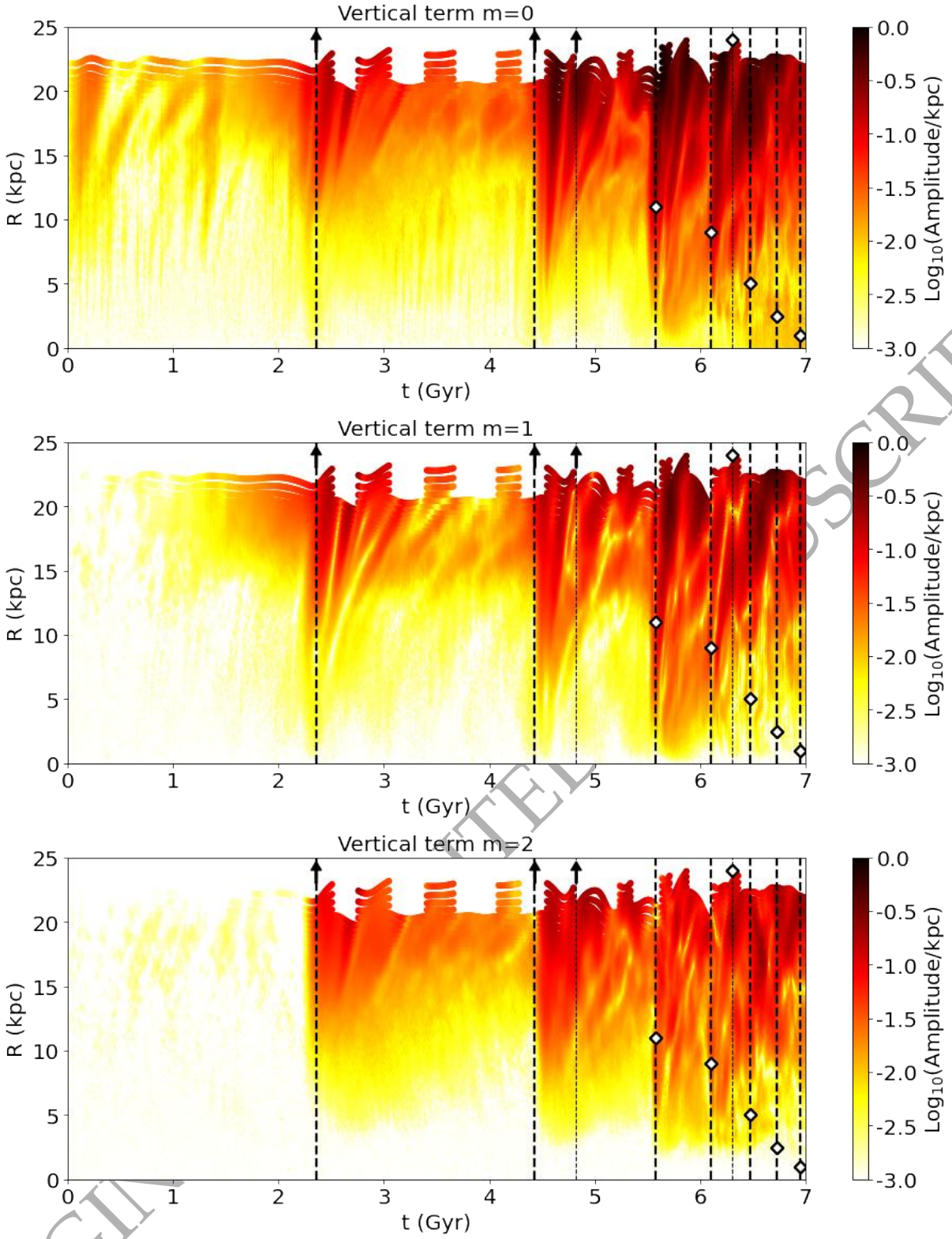

Figure 5. Amplitude of the Fourier vertical terms m=0 (upper panel), m=1 (middle panel) and m=2 (lower panel). Dashed vertical lines, arrows and white diamonds are as in Figure 4.

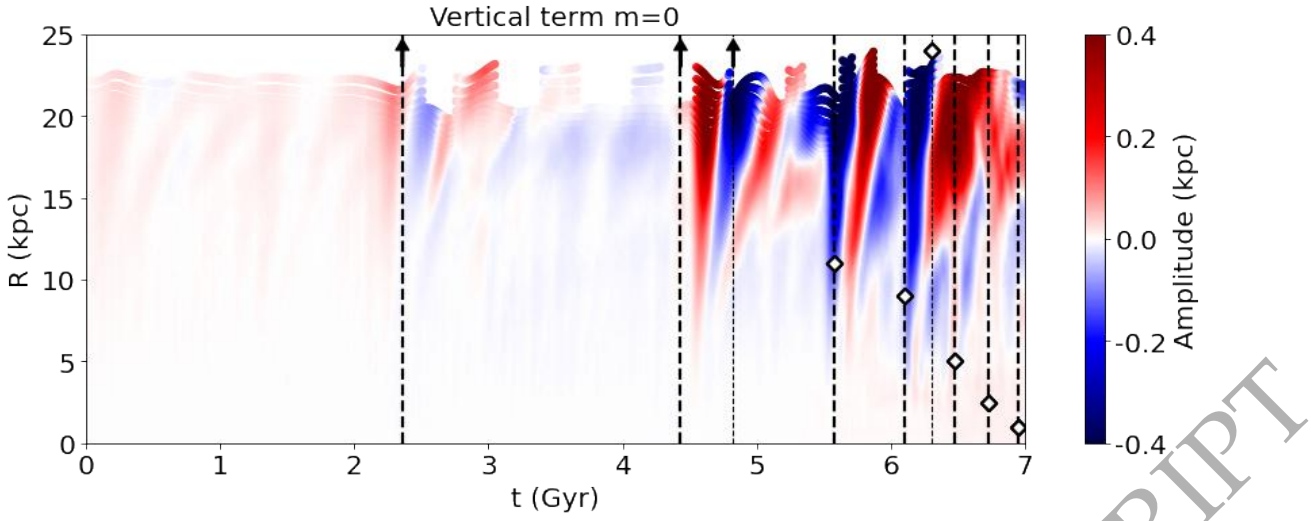

Figure 6. Amplitude of the vertical Fourier m=0 term. Dashed vertical lines, arrows and white diamonds are as in Figure 4.

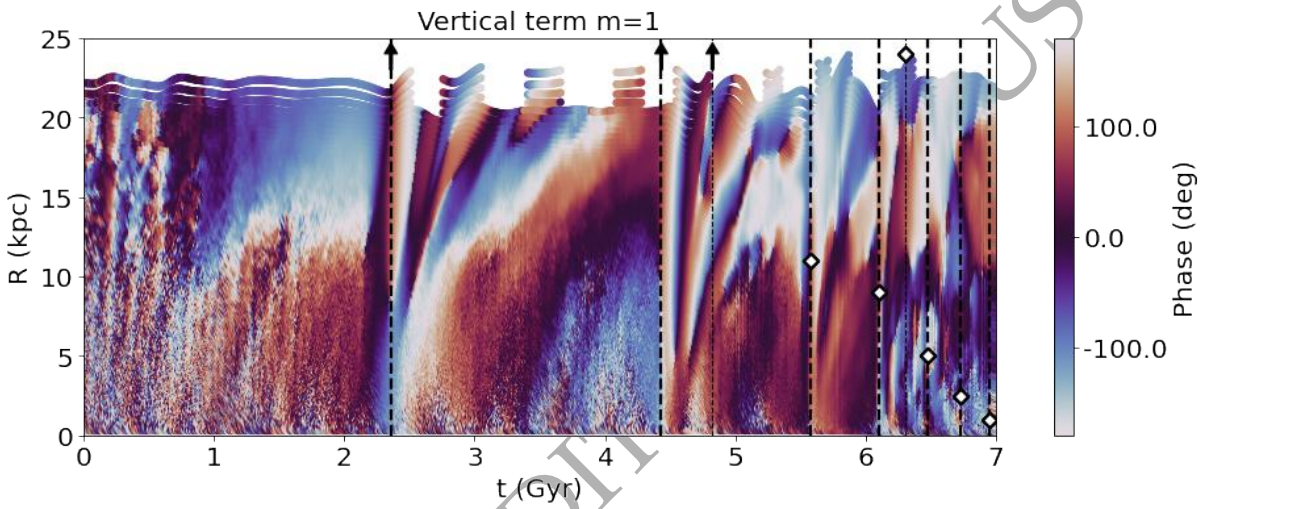

Figure 7. Evolution of the phase angle for the m=1 Fourier term. Dashed vertical lines, arrows and white diamonds are as in Figure 4. A zoom of the last region is given in the Appendix (Figure B1).

The first plane-crossing of Sgr brings the above-described pattern to an end. The interaction with Sgr resets the phase angle at all radii, and causes the outer parts of the disc ($R \gtrapprox 8$ kpc) to precess (term used in literature to indicate the variation of the line of nodes) in a fast and almost rigid way in the same (prograde) direction with respect to Galactic rotation. At 15 kpc, the prograde behaviour is maintained for about 200 Myr. Right after, abrupt variations of the phase angle take place, corresponding to the oscillatory behaviour observed in Section 4.2.1 (i.e. disc flapping). Visually, $m = 1$ prograde distortions with a different orientation (i.e. phase angle) with respect to those in the outer parts appear to originate from the inner parts and move to the outer parts of the disc. In contrast, the inner parts of the disc ($R \lessapprox 8$ kpc) exhibit a retrograde precession, which is progressively restored also in the outer parts of the disc, as soon as the perturbation caused by the interaction is damped over the course of time. Therefore, Regime 1 is characterized by a slow recovery from the first interaction with Sgr, where the disc progressively goes back to a slow, retrograde, differential pattern speed. Also in this case, the line-of-nodes progressively winds up into a leading spiral.

The second plane-crossing of Sgr (which, in this case, approximately coincides with its second pericentric passage) marks the end of Regime 1. From this point on, time scales become faster, and features are often not coherent over all Galactic radii. It is therefore convenient to zoom in the last region, as shown in Figure B2 (top).

At about 4.5 Gyr, after Sgr' second plane-crossing, most of the disc ($R > 5$ kpc) exhibit a fast, prograde and almost rigid precession, in agreement with what was observed during the first interaction. Between 10 and 20 kpc, the average period (i.e. time required for the line-of-nodes to make one complete rotation around the Galactic center) is of about 300 to 400 Myr, corresponding to an angular speed of about 20 km/s/kpc. (This information can be approximately obtained from Figure B2 by estimating the time difference between two recurrences of the same phase angle. However, pattern speeds will be more extensively discussed in the following Sections.)

Between 5.5 and 6.1 Gyr, the outer parts of the disc respond

to the impact of Sgr in a similar way to the interactions described before, while the inner parts seem to develop the slow, retrograde pattern observed in Regimes 0 and 1 after about 5.7 Gyr. This situation represents an illustrative example of how different regimes may co-exists at the same time, due to different dynamical time-scales in the Galactic disc. Indeed, here the time interval between two impacts is of the same order of the disc dynamical times in the outer disc (Regime 2), but still larger than those in the inner disc (Regime 1).

After 6.1 Gyr, plane-crossings occur so frequently that the disc is continuosly subjected to external perturbations. As a consequence, complicated and discontinous patterns arise in the disc, being clearly visible also in the inner regions, in which Sgr is progressively being absorbed. In the outer disc (≈ 10 - 20 kpc), a coherent structure survives from about 6.2 to 6.7 Gyr, showing a relatively fast, prograde and nearly rigid precession, completing half of the disc (180 deg) in about 300 Myr (roughly corresponding to an angular speed of ≈ 10 km/s/kpc). Similarly, other features may survive for a few hundreds of Myr, but they do not remain coherent for more than a few kpc in Galactic radius. Therefore, the recurrent impacts on a short time-scale, together with the proximity of the satellite, make Regime 3 the most perturbed regime analyzed in this work, dominated by complex disc patterns, which do not remain coherent for very long, both in space and time.

A visual representation of the $m = 1$ slow retrograde pattern, typical of quiescent phases, can be seen in Figure A2. The $m = 1$ prograde pattern, which occurs during an interaction, can be visualised in Figure 3 and A3.

4.2.4 *Fourier vertical term m=2*

The m=2 term corresponds to a bi-symmetric vertical distortion of the Galactic disc. In general, its temporal evolution presents some relevant differences from the previously discussed $m = 1$. For example, $m = 2$ is completely absent in the pre-interaction regime, and gets excited by the first plane crossing of Sgr (at ≈ 2.3 Gyr), as shown by Figure 5.

The temporal evolution of the $m = 2$ phase angle is shown in Figure 8 (see also Figure B2, which is zoomed in the most perturbed region). As we can see, the $m = 2$ term exhibits a very regular behaviour. Even in the latest regimes, where Sgr's impacts become more frequent and the disc is strongly perturbed, the $m = 2$ pattern can be roughly recognised. For comparison, the m=1 term appears to be much more fragile and easily disrupted.

As will be better explained in the spectral analysis, the $m = 2$ bending waves typically move in a prograde direction (also in quiescent phases, unlike $m = 1$). Their angular speeds show a very mild variation with radius, which causes the bending waves to wrap up very slowly. Starting from an initially long radial wavelength (> 25 kpc), the phase of the m=2 term progressively winds up, reaching a radial wavelength of ≈ 8 kpc almost 2 Gyr after the latest interaction. Therefore, the pitch angle of the m=2 vertical wave can, in principle, be used as a clock to date the most recent interaction.

During a plane-crossing, if that also coincides with a pericentric passage, the phase-angle of the m=2 term gets reset at all radii, and, intially straight, moves in a prograde direction, similarly to what observed for the $m = 1$ term. Figure 9 shows the difference between the phase angle of the $m = 1$ and the $m = 2$ term (ϕ_1 and ϕ_2, respectively) at different times. During the first two pericenters, the $m = 1$ and the $m = 2$ term seem to be somewhat aligned, moving at approximately the same speed (i.e. their difference is roughly constant). Such behaviour might be due to a coupling between the Fourier terms, which occurs as a response to the interaction with Sgr. However, this effect becomes less clear in the latest and more perturbed regimes, where the presence of Sgr inside the disc does not allow coherent features to survive for more than a few kpc in Galactic radius. In contrast, very regular patterns can be observed in quiescent regions (e.g. 3 < t < 4.4 Gyr), where the two Fourier terms revolve at their own typical speed, with the $m = 1$ being slightly retrograde (see above) and the $m = 2$ typically prograde. This difference is causing the difference $\phi_1 - \phi_2$ to be decreasing with time.

4.2.5 *Spectral analysis*

Originally developed for density waves (Sellwood & Athanassoula 1986; Masset & Tagger 1997; Quillen et al. 2011; D'Onghia & L. Aguerri 2020), spectral analysis has been recently extended to bending waves (Chequers et al. 2018; Chequers & Widrow 2017), allowing us to describe them in terms of frequency power spectrum as a function of Galactocentric radius. A full description of vertical spectrograms can be found in Chequers et al. (2018); Chequers & Widrow (2017), and technical details are given in Appendix D. In this paper, we will use vertical spectrograms to identify the most relevant features over a given time baseline. Specifically, we will be interested in determining the angular speed (i.e. temporal variation of the phase angle $\Phi_m(R)$, see Equation 1) of the most relevant Fourier vertical terms $m \geq 1$ in different regimes of interaction with Sgr.

Figure 10 consists of six vertical spectrograms, showing the frequency spectrum for $m = 1$ bending waves in different periods of the simulation. To relate the vertical response of the disc to the satellite's orbit, we chose a temporal baseline of 1 Gyr for each spectrogram, which implies a resolution on the vertical axis of 6.28 km/s/kpc (the temporal resolution of the simulation is 10 Myrs). (For a sharper resolution on the vertical axis, implying a longer baseline, see Appendix D.) One of the most obvious features of Figure 10 is that the power reaches typically larger values (i.e. stronger bending waves) in the spectrograms where one (or more) interaction(s) with Sgr occurred (panels marked by a black star), whereas it remains relatively low in quiescent regions (panels A and C).

It is also instructive to look at where the power is concentrated at different stages of the Milky Way-satellite interaction. In quiescent regions, most of the power is concentrated close to angular speed 0 (panel A), or slightly retrograde values (panel C), in the outer regions of the disc. This approximately aligns with the vertical resonance $\Omega - \nu_z$, where Ω is the angular rotation rate of the Galaxy and ν_z is the vertical epyciclic frequency. This is the so-called slow wave, and is expected to be retrograde because, in a flattened galaxy, the vertical frequency $\nu_z > \Omega$. The slow and retrograde bending wave has been already discussed in the literature (Binney & Tremaine 2008; Chequers & Widrow 2017; Chequers et al. 2018).

However, in panel B, power is located in two main regions: one close to ≃20-25 km/s/kpc, indicating the prograde precession associated with Sgr's impact, and the slow retrograde precession, which is visible before/after the effects of the perturbation have relaxed. The prograde feature disappears in panel C, where no interaction take place. Therefore, there is a clear connection between the vertical pattern speeds in the Galactic disc and the satellite's orbit. This is further confirmed by panels D, E and F, where multiple interactions are present, and transient prograde features become prominent. We also observe that prograde angular speeds in panel E and F are typically slower than those in panel B and D.

Figure 11 repeats the vertical spectrograms of Figure 10, but

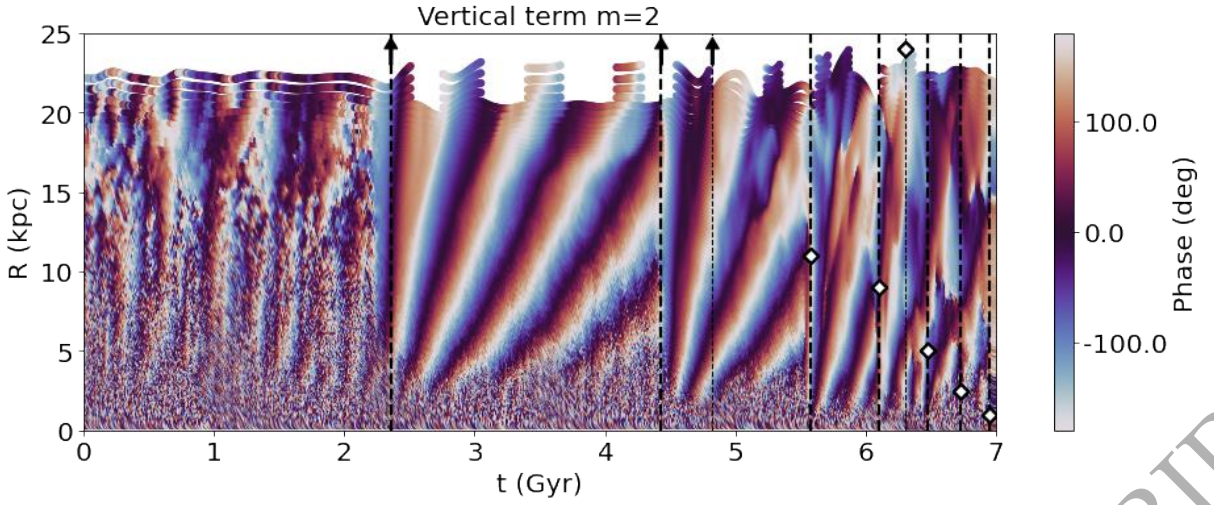

Figure 8. Evolution of the phase angle for the m=2 Fourier term. Dashed vertical lines, arrows and white diamonds are as in Figure 4. A zoom of the last region is given in the Appendix (Figure B1).

now for the $m = 2$ term. Considerations similar to the ones above can be done here, with the difference that: (i) the m=2 term is completely absent before the first interaction (panel A), and (ii) the resonance curves are different, as the angular speed $\omega = m\Omega \pm \nu_z$, with $\omega = m\Omega_p$, where Ω_p is the pattern speed of the bending wave. In the previous sections, we found that $m = 2$ bending waves present a very regular behaviour, characterized by a prograde angular speed. Indeed, the spectrograms indicate that, in the outer regions, the power aligns with the vertical resonance at $\omega = m\Omega - \nu_z$ (see Bland-Hawthorn & Tepper-Garcia 2020), which demarcates a prograde angular speed.

4.2.6 *Relating response in different dimensions*

Figure 12 shows the phase angle of the $m = 2$ vertical term (Z) as a function of Galactocentric radius R, compared to other quantities that might be of interest. The $m = 2$ term in vertical velocity (V_z) appear to be typically shifted by 90 deg with respect to the $m = 2$ phase in Z, as expected from a wave-like motion.

When comparing the $m = 2$ vertical term (Z) and the $m = 2$ spiral arms in density, we find that, in general, there is no obvious correlation. This can be also seen in Figure 2, where the spiral arms in density appear more tightly wound than the ones in the vertical spiral wave. Indeed, such behaviour is somewhat expected, as the $m = 2$ density and bending waves have, respectively, a pattern speed of $\Omega(R) - \kappa/2$ and $\Omega(R) - \nu_z/2$. This is in good agreement with the recent analysis presented by Bland-Hawthorn & Tepper-Garcia (2020).

Figure 13 shows the angular difference between the $m = 2$ phase angle in density and in Z as a function of time for different Galactocentric radii. As we can see, the $m = 2$ density and bending waves usually move at their own typical rate, with the $m = 2$ in density wave being typically faster than $m = 2$ in Z. This is apparent when the difference ϕ_2 (Density) - ϕ_2 (Z) increases as a function of time. However, in proximity of an interaction, the behaviour is different. The $m = 2$ density and bending waves tend to align, and move at a similar speed for a very short time. This behaviour might highlight a resonance, caused by the interaction with Sgr.

5 OBSERVING THE DISC RESPONSE

The previous Section showed that the evolution of the Galactic disc and the orbit of a perturbing satellite are tightly correlated, thereby leading to various expectations for vertical pattern speeds in the Galactic disc and other quantifiable properties, depending on the status of interaction. In principle, the response of the disc can be inferred from observations, and used to learn more on the interaction with the perturbing satellite(s) and the perturbed halo.

The evolution of the disc in N-body simulations can be deduced by comparing subsequent snapshots at different times (as was done in the previous Section). However, in real data, observations provide us with positions and velocities of stars in the Galaxy only at the present time. Therefore, a method is required to infer the actual behaviour of the disc using only the instantaneous measurements of the 6-dimensional phase-space of stars.

In this Section, we aim to mimic the real data approach, in order to understand whether it is possible to recover the actual instantaneous behaviour of the Galactic disc by simply analysing positions and velocities of stars at a given time. Certainly, the equations governing the vertical response of the Galaxy to the recurrent impacts of a satellite galaxy should be based on a deep dynamical investigation, which is beyond the scopes of the present paper. Instead, here we use a very simple kinematical approach, and test its validity and limitations. The approach currently includes the three Fourier vertical terms $m = 0$, 1 and 2 (Appendix A shows that this is a reasonable approximation), but it can be easily extended to other Fourier terms, if needed. We model the disc using an exponential vertical profile, whose vertical displacement is determined as follows. For a given R, the amplitude h_0 of the $m = 0$ vertical term is free to change with time. The two vertical terms $m = 1$ and $m = 2$ have a time-varying amplitude (h_1 and h_2, respectively) and phase (ϕ_1 and ϕ_2, respectively). The above time-dependent vertical displacement has implications on the vertical velocities of the stars, whose mean trend can be calculated using the Collisionless Boltzmann Equation (see Equation 6 and its derivation for the $m = 1$ term in Poggio et al.

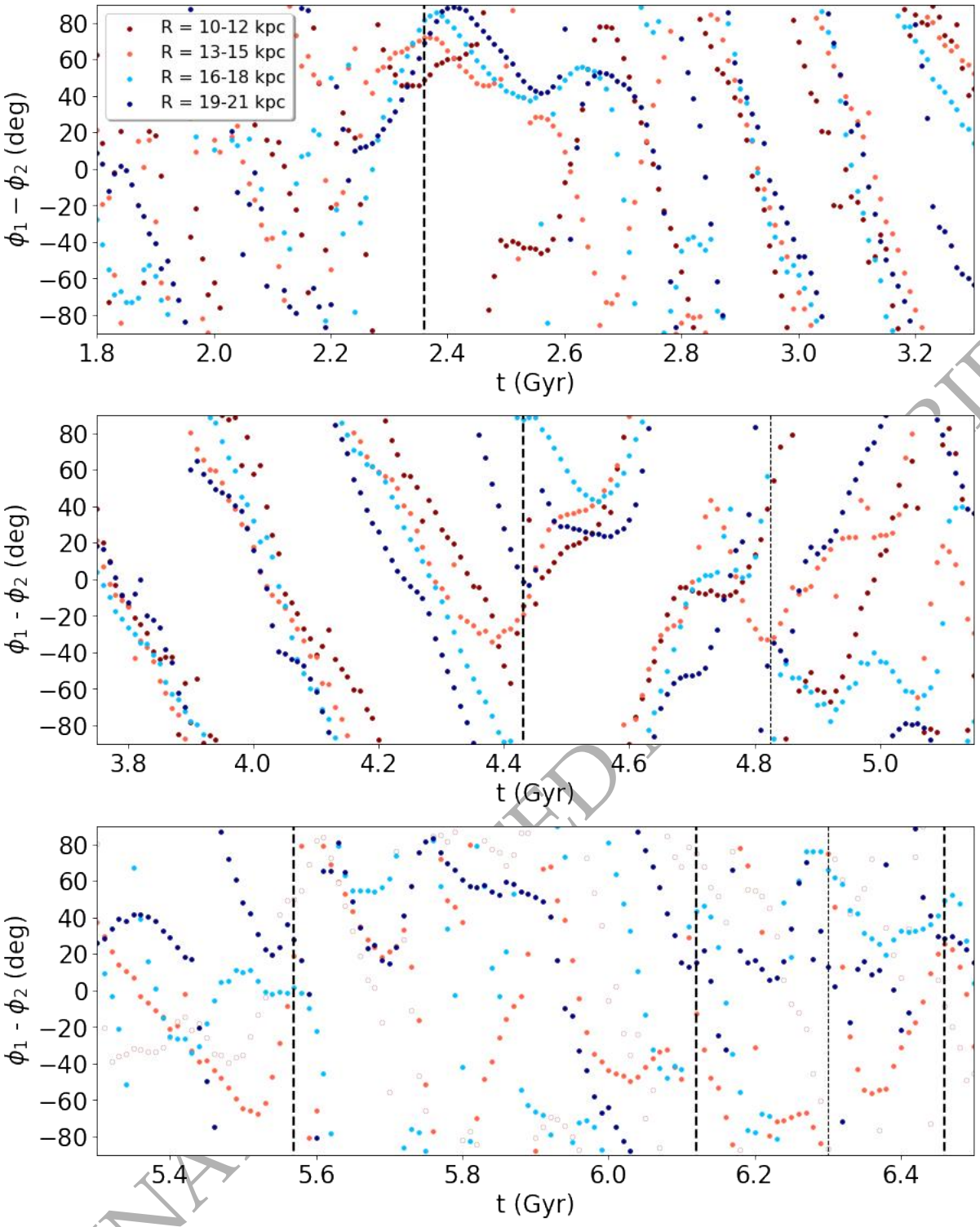

Figure 9. Difference between the phase angle of the m=1 and m=2 Fourier terms at different Galactocentric radii R. Dashed vertical lines as in Figure 4. Close to interactions, the two terms are moving at the same speed (i.e. where the difference is constant), illustrating the coupling of the Fourier terms. In the bottom panel, the phase angle inside 12 kpc are represented as open symbols, to avoid crowding.

2020):

$$V_z(R,\phi) = \frac{\partial h_0}{\partial t} + \Big(\frac{V_\phi}{R} - \frac{\partial \phi_1}{\partial t}\Big) h_1 \cos(\phi - \phi_1) + \frac{\partial h_1}{\partial t} \sin(\phi - \phi_1) + \Big(2\frac{V_\phi}{R} - \frac{\partial \phi_2}{\partial t}\Big) h_2 \cos(2\phi - \phi_2) + \frac{\partial h_2}{\partial t} \sin(2\phi - \phi_2) \quad , \tag{2}$$

where the kinematic parameters $\frac{\partial \phi_1}{\partial t}$ and $\frac{\partial \phi_2}{\partial t}$ are the angular frequencies of the $m = 1$ and $m = 2$ terms, respectively, and $\frac{\partial h_0}{\partial t}$, $\frac{\partial h_1}{\partial t}$, $\frac{\partial h_2}{\partial t}$ are the amplitude variations of the corresponding Fourier

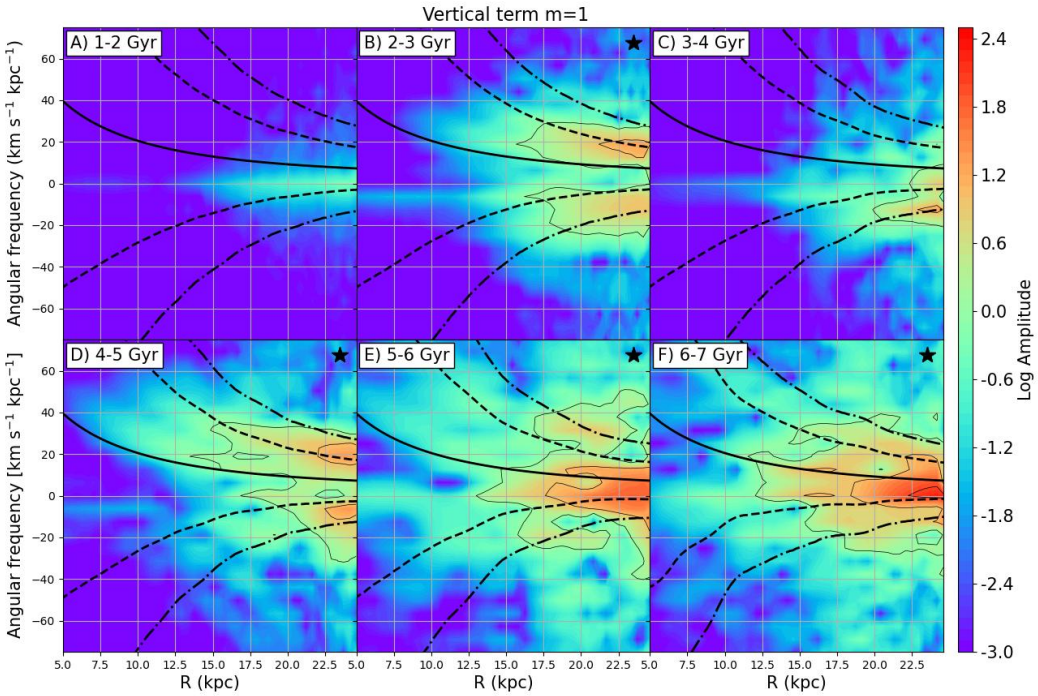

Figure 10. Vertical spectrograms of the Fourier m=1 vertical term. Each panel covers a temporal bin of 1 Gyr in the simulation. Panels marked by a black star are those where one (or more) interaction(s) with Sgr took place. The solid curve shows corotation. The dashed curves show the vertical resonances at $\Omega(R) \pm \nu_z(R)$, where $\Omega(R)$ is Galactic rotation and $\nu_z(R)$ is the vertical frequency (see Appendix). The dashed-dotted curves show the vertical resonances at $\Omega(R) \pm 2\nu_z(R)$. The thin solid lines show the countour levels Log(Amplitude)=0, 1 and 2.

terms. These five parameters are, in general, non-zero, and can be statistically inferred using positions and velocities (R, ϕ, V_ϕ, V_z) of the stars in the Galactic disc at a given time using Equation 2. To do this, in this experiment we use a simple non-linear least squares method, assuming that the (spatial) amplitudes and phases of the $m = 0, 1$ and 2 vertical terms are known. Hereafter, we will refer to this method as the *Instantaneous measurement*, since the kinematic parameters are recovered from the 6-dimensional phase-space information for stars at a fixed time, as in the case of real data.

As anticipated above, an alternative way to determine the instantaneous evolution of the Galactic disc is to compare the amplitudes and phases at different snapshots. For example, one can calculate the angular speed $\frac{\partial \phi_1}{\partial t}$ at given radius R by naively taking the phase difference at two subsequent snapshots. Alternatively, one might use the vertical spectrograms (see Section 4.2.5), which, however, provide us with the power distribution on a relatively large time-scale (1 Gyr), due to the simulation temporal resolution. Therefore, in this simple experiment, we use the first approach, and name it *Differential Fourier analysis*.

Figure 14 shows the results obtained when recovering the angular speeds $\frac{\partial \phi_1}{\partial t}$ and $\frac{\partial \phi_2}{\partial t}$ of the $m = 1$ and $m = 2$ vertical terms according to the Instantaneous measurement and the Differential Fourier analysis at different Galactic radii. In this experiment, the reliability of the two methods is assumed to be similar. The Differential Fourier Analysis, which in principle is the most simple and straightforward approach one can use, appears to be intrinsically noisy, and exhibit considerable variations on a short time-scale compared to the Instantaneous method. On the other hand, the Instantaneous method relies on a very simple approach, which presumably does not capture all the physical processes at work in the Galaxy. Notwithstanding their considerable differences, the two methods appear to produce results in rough agreement with each other. As we can see from Figure 14, this occurs even in the latest regimes, where the disc is more perturbed. Nevertheless, some discrepancies remain. These may be due to local disturbances that deviate from the global pattern (see for example Figure B2), possibly induced by rapid variations of the potential following an interaction. In this case, short-time disturbances could be presumably detected by the Differential Fourier Analysis, whereas the Instantaneous method would be more prone to map long-term variations, being based on stellar velocities. This possible interpretation will be further explored in future works.

Figure 14 shows that Sgr's passages trigger bumps in the observed angular speeds. Such behaviour is not limited to the temporal range shown in the Figure, but it is also observed during other interactions, in agreement with what would be expected based on Figure 10.

However, a realistic magnitude limited survey does not cover the entire Galactic disc. Therefore, we perform an additional experiment, to test the applicability of the data-like approach on a limited portion of the Galactic disc. We place the simulated Sun at 12 kpc from the Galactic center, to approximately reproduce a realistic warp amplitude based on the observed mean vertical displacement at a given heliocentric distance (e.g. Momany et al. 2006). While the Sun's distance from the Galactic center is maintained fixed, we

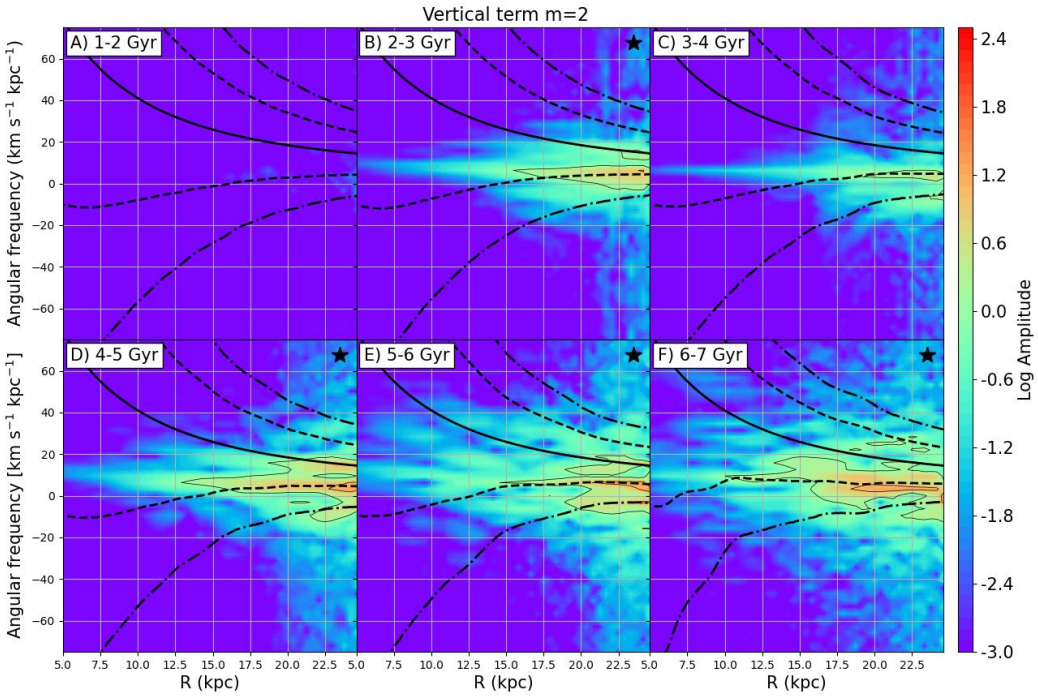

Figure 11. Same as Figure 10, but for the Fourier m=2 vertical term.

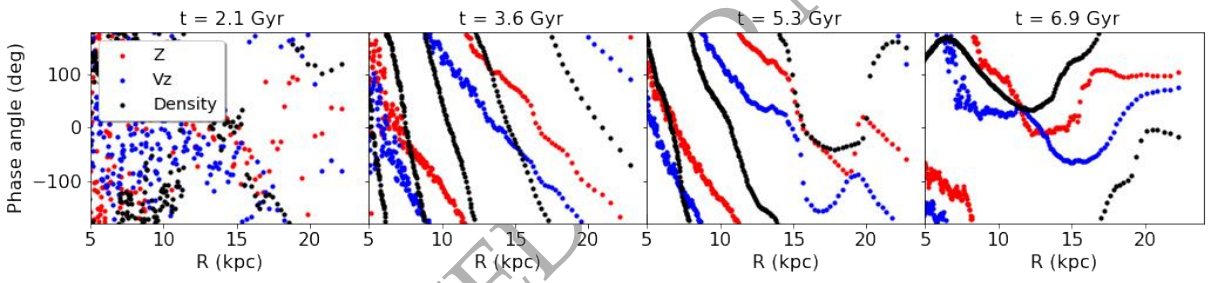

Figure 12. Comparison between the phase angle of the m=2 mode for Z (red), Vz (blue) and density (black) at t=3.3 Gyr, 5.5 Gyr and 6.5 Gyr (from left to right).

place the Sun at 8 different azimuthal angles (spaced by 45^o) for a given snapshot. Then, we select only stars within 10 kpc from the Sun, to approximately mimic a Gaia DR3-like sample of stars. For each snapshot, we end up with 8 mock catalogs of stars, containing $\simeq$ 600 000 particles (which implies a lower statistic than the one that can presumably be reached with Gaia DR3). Due to the low statistics, in this second experiment we fit for a single value of angular speed $\frac{\partial \phi_1}{\partial t}$ and $\frac{\partial \phi_2}{\partial t}$, instead of evaluating each radial ring separately. (This approximation is equivalent to averaging over the portion of the disc covered by the mock dataset.) Finally, we take the median of the results from the 8 mock catalogs, and calculate the dispersion around the median value, and repeat the procedure for all the snapshots of interest. The results are presented in Figure 15. As we can see, the dispersion can be significant in some places, as expected, due to the complexity of the physical mechanisms at work in our Galaxy, which are presumably not captured by our simple approach. However, the median value is in good agreement with the values obtained using the entire disc, meaning that the approach is unbiased.

6 DISCUSSION AND CONCLUSION

6.1 Key results

Using N-body simulations from L18, we have described the interaction between the Milky Way and Sgr in terms of four different interaction regimes (called Regime 0,1,2,3), based on the orbital history of Sgr and the dynamical time scales in the Galactic disc. Each regime dictates the properties, extent and evolution of the disc perturbations. We have quantitatively characterised the evolution of the vertical distortions of the disc under the repeated impacts of Sgr using Fourier decomposition and spectral analysis. Some of the

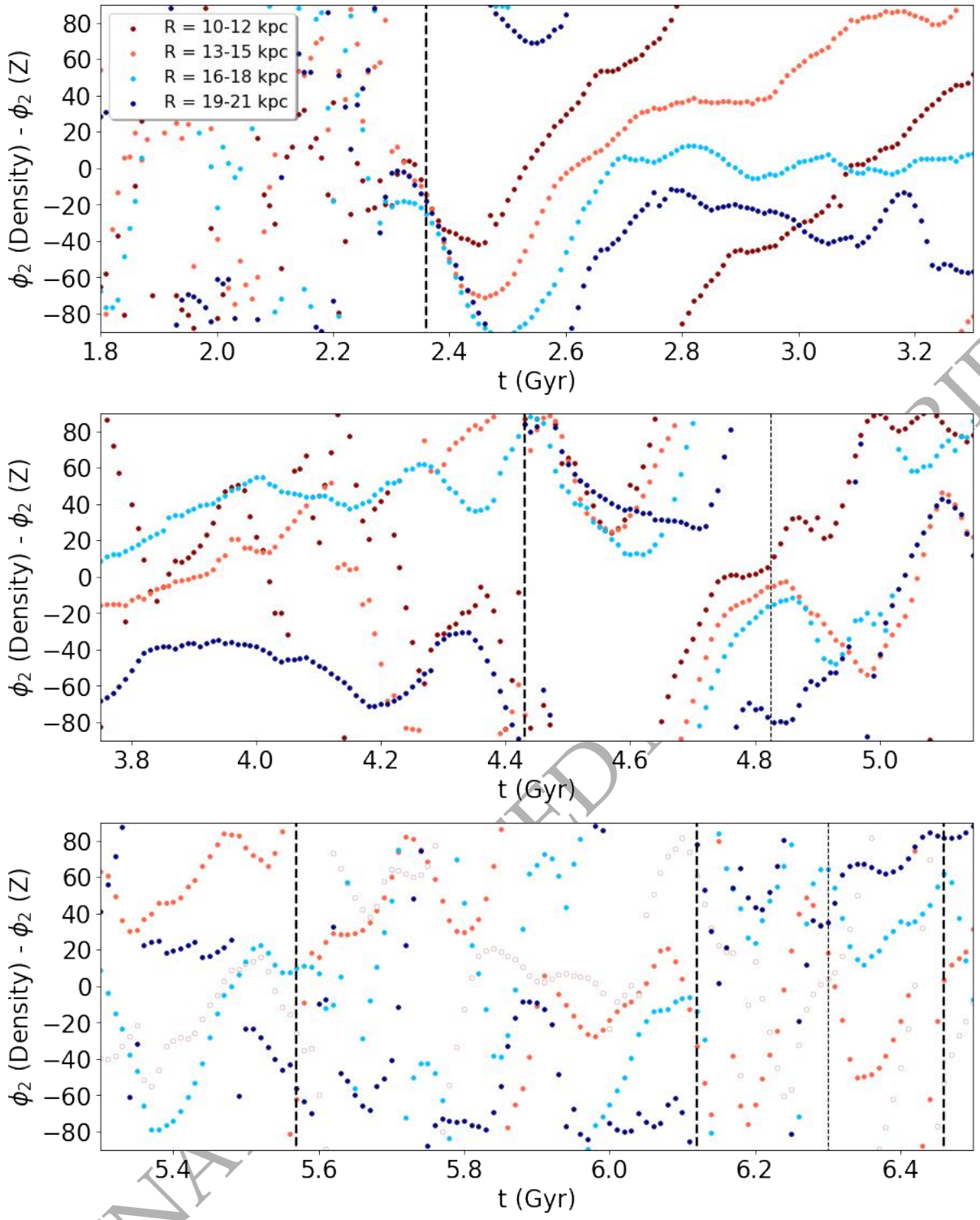

Figure 13. Same as Figure 9, but showing the difference between the m=2 density and m=2 vertical Fourier terms.

observed features have been already discussed in literature, while others are new. Finally, we have tested the validity of pattern speed measurements in a realistic model. The main results of the paper are summarized below:

(1) The $m = 0$ term manifests itself as a ring-like vertical distortion with alternate sign propagating from the inner to the outer parts of the disc. The radial propagation speed is faster after an interaction, and becomes much slower (almost static) in quiescent phases.

(2) The $m = 1$ vertical term is characterized by a slow, differential, retrograde precession in the quiescent regimes, while it moves in a relatively fast and prograde direction in the last regimes or close to an interaction.

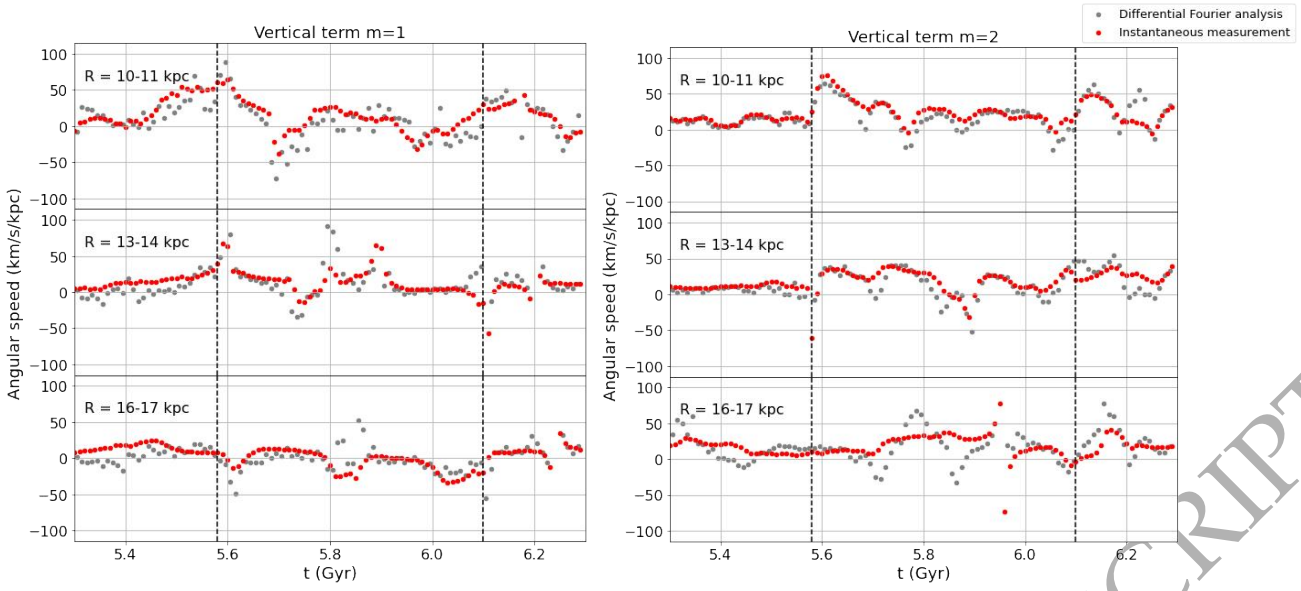

Figure 14. Comparison between the angular speed obtained from a data-like approach i.e. instantaneous method, see Section 5; red points) and the Diffential Fourier analysis (grey points) for the m=1 (left) and m=2 (right) Fourier vertical terms. Different rows refer to different positions in the Galactic disc. The grey points are obtained by simply subtracting the phase angles at two subsequent snapshots (for a more sophisticated approach, see Section 4). For the instantaneous method, formal uncertainties are of about 2-3 km/s/kpc or less, and therefore too small to be seen in the plot.

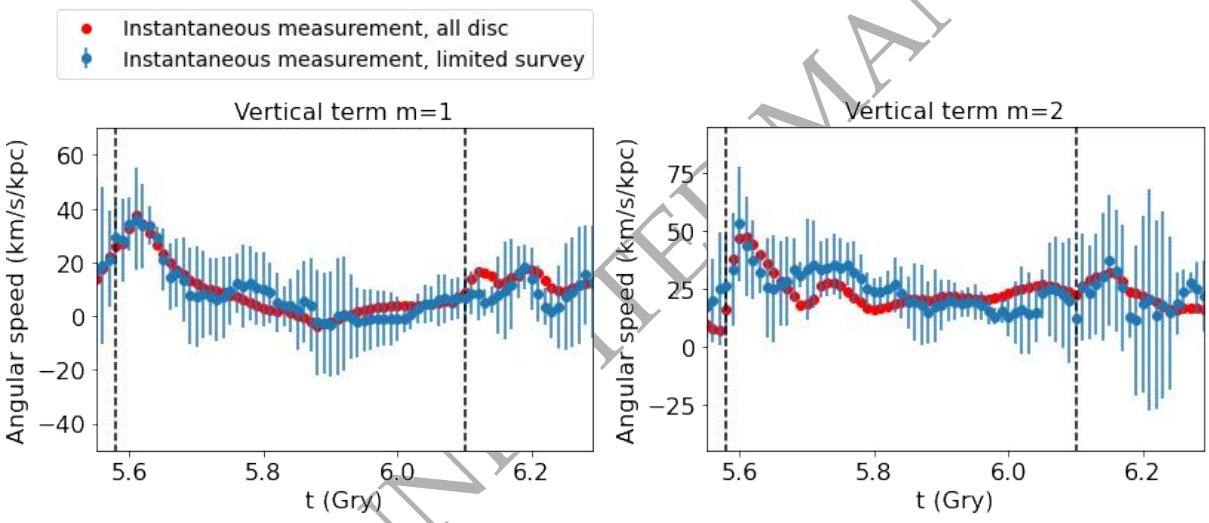

Figure 15. Same as Figure 14, but comparing the results of the data-like approach using the entire disc (red points) and a limited volume of the Galactic disc (blue points). For a given snapshot, the blue points show the median angular speed obtained from eight different volumes (see text), while the error bar shows the median absolute deviation (MAD) of the obtained values.

(3) The $m = 2$ vertical term is excited by the first interaction with Sgr, and presents a very regular behaviour, apparent as a prograde bi-symmetric trailing spiral, which progressively winds up with time after an interaction.

(4) In quiescent phases, the Fourier vertical terms $m = 1$ and $m = 2$ revolve at their own typical rate, which is determined by vertical Lindblad resonances. However, their angular frequency is forced to change during the interactions with Sgr, and they both move in a prograde direction for a few hundred Myrs, at approximately the same speed. Such coherent motion might perhaps indicate a resonance, which is arising as a response of the disc to the interaction with the satellite.

(5) The instantaneous evolutionary state of the Galactic disc can be parameterised using the amplitude and phase angle variation (angular speed) of the Fourier vertical terms. Such parameters can be recovered in an unbiased way from stellar positions and velocities in the Galactic disc at a given time (i.e. similar to the real data case).

6.2 Implications

In this work, we have shown that the $m = 0$, 1 and 2 Fourier vertical terms dominate and behave in a different way in distinct phases of the interaction process with a satellite galaxy. Although some caveats (discussed below) should be kept in mind, our results imply

that *the kinematic parameters describing the instantaneous vertical evolution of the Galactic disc have a constraining power on the dynamical state of the interaction*, when a Milky Way-Sgr like accretion is considered. Taking advantage of current and future datasets, which allow us to characterize the Galactic disc on an unprecedentedly large volume, one can (i) place observational constraints on the evolution of the perturbed Galactic disc, and (ii) use high-resolution N-body simulations to bridge the gap between observation and theory, to suggest a possible dynamical interpretation of the observations in the context of a Milky Way-Sgr interaction.

The scenario analysed in this work provides a possible framework for the interpretation of measurable quantities, such as the pattern speed of the Galactic warp. Here we find that a fast and positive value of warp pattern speed, such as measured for the Milky Way using *Gaia* data by Poggio et al. (2020); Cheng et al. (2020), can only be obtained during or after interactions. In this context, the warp pattern speed can be used to constrain the current interaction regime of the Milky Way, as the simulations show that a fast and prograde warp precession rate is a natural consequence of an interaction (and a typical behaviour during the second and third regimes, where interactions are more frequent, see Figure 10E, 10F).

Additional measurements can potentially give further insights into the origin of vertical disturbances and relate to satellite contribution. For example, the pattern speed of the $m = 2$ vertical term might be measured using future datasets. Such result would be not only interesting by itself, but also because the difference between the angular speed of the m=1 and m=2 terms might represent a complementary way of determining if an interaction has occurred in the last few hundreds of Myrs. Additionally, given that the $m = 2$ mode is persistent and winds-up very slowly (see Fig. 8), its pitch angle, even measured locally, may provide a good clock for measuring the time since the last perturbation.

6.3 Limitations and future prospects

This work aims to make further progress towards the understanding of the vertical response of the disc to the recent accretion history of the Galaxy. As a starting point, we analysed the response to the repeated impacts of a Sgr-like satellite. However, a number of caveats should be kept in mind, when interpreting our results in their wider context. For instance, modelling Sgr orbital history from the virial radius crossing to the present-day is notoriously difficult, which is further exacerbated by the large uncertainties on its parameters (e.g. progenitor mass profile, last pericentric passage, etc.), and those of the Milky Way's own potential. Hence, instead of aiming to reproduce the *exact* orbital history of Sgr and the *exact* vertical response of the disc, we have rather concentrated ourselves on the exploration of the physical spatial reaction to (and the relative time-scales of) an interaction between a Milky Way-like galaxy and a Sgr-like satellite. In addition to this, it should be noted that the Magellanic Clouds also play a role in generating vertical pattern speeds in the Galactic disc (e.g. Weinberg & Blitz 2006; Laporte et al. 2018a). Its effect in combination with Sgr was already explored in Laporte et al. (2018b) showing that the recent interaction with the LMC modulates the response due to Sgr which is particularly noticeable in the outer disc ($\geq$ 16 kpc). In addition to this, we note that the simulation does not include a gaseous component, which might contribute to the bending wave damping. A deeper exploration is left for future work.

Finally, it should be mentioned that our work did not consider the eïňĂects of bar buckling. In their N-body experiments, Łokas (2019) shows that disc vertical displacement induced by the bar buckling can reach a maximum value of about $\approx$ 0.8 kpc at about 2 times the disc scale length for the first buckling, and of about 0.6 – 0.7 kpc at $\approx$ 3 times the disc scale length for the second buckling. These displacements would be comparable (negligible) in strength to satellite-induced ones in the inner (outer) disc. Whether such effects play a major role in shaping the vertical distortions in the Milky Way at present is less clear. The different fractions of stellar population making up the bar (Ness et al. 2013; Zoccali et al. 2017; Wylie et al. 2021) suggest the bar could not have formed in the last 3 Gyrs (see Debattista et al. 2019). Instead, observations of Miras towards the central part of the Galaxy suggest that bar formation happened 8-9 Gyr ago (Grady et al. 2020). Although the aforementioned study suggests this happened through bar buckling, it should be noted that this is not the sole mechanism which can produce an X-shape bar (e.g. see Sellwood & Gerhard 2020; Baba et al. 2021). Nevertheless, it would still be interesting to explore more generally how bar buckling would interfere with the vertical disturbances induced by satellite interactions. Future works comparing observational constrains on the disc vertical evolution with possibly more sophisticated dynamical models will certainly reveal further information on the recent accretion history of the Milky Way.

ACKNOWLEDGEMENTS

We thank the anonymous referee for helpful comments, and Larry Widrow for useful discussions. EP acknowledges financial support from the Center of Computational Astrophysics, Flatiron Institute (New York, USA), which enabled a long-term visit in 2019 to develop this project. CL thanks the Observatoire de la Côte d'Azur for hosting him on a long-term visit. This work used the Extreme Science and Engineering Discovery Environment (XSEDE), which is supported by National Science Foundation grant number OCI-1053575. This work was supported in part by World Premier International Research Center Initiative (WPI Initiative), MEXT, Japan. EP acknowledges the partial support of ASI through contract ASI 2018-24-HH.0, Gaia Mission - The Italian Participation to DPAC. CL acknowledges funding from the European Research Council (ERC) under the European UnionâĂŹs Horizon 2020 research and innovation programme (grant agreement No. 852839). KVJ and DF were supported by NSF grant AST-1715582 EP acknowledges support from the Centre national d'ĂĽtudes spatiales (CNES).

DATA AVAILABILITY STATEMENT

The data presented in figures will be shared on reasonable request to the corresponding author. Raw simulation data can be shared on reasonable request to the original team (Laporte et al. 2018b).

REFERENCES

Antoja T., et al., 2018, Nature, 561, 360
Aumer M., White S. D. M., 2013, MNRAS, 428, 1055
Baba J., Kawata D., Schönrich R., 2021, arXiv e-prints, p. arXiv:2104.09526
Bailin J., 2003, ApJ, 583, L79
Belokurov V., Erkal D., Evans N. W., Koposov S. E., Deason A. J., 2018, MNRAS, 478, 611
Bergemann M., et al., 2018, Nature, 555, 334
Binney J., 2012, MNRAS, 426, 1324
Binney J., Schönrich R., 2018, MNRAS, 481, 1501
Binney J., Tremaine S., 2008, Galactic Dynamics: Second Edition

Bland-Hawthorn J., Tepper-Garcia T., 2020, arXiv e-prints, p. arXiv:2009.02434
Bland-Hawthorn J., et al., 2019, MNRAS, 486, 1167
Blumenthal G. R., Faber S. M., Flores R., Primack J. R., 1986, ApJ, 301, 27
Burke B. F., 1957, AJ, 62, 90
Carlin J. L., et al., 2013, ApJ, 777, L5
Carrillo I., et al., 2019, MNRAS, 490, 797
Chen X., Wang S., Deng L., de Grijs R., Liu C., Tian H., 2019, Nature Astronomy, 3, 320
Cheng X., et al., 2020, arXiv e-prints, p. arXiv:2010.10398
Chequers M. H., Widrow L. M., 2017, MNRAS, 472, 2751
Chequers M. H., Widrow L. M., Darling K., 2018, MNRAS, 480, 4244
D'Onghia E., L. Aguerri J. A., 2020, ApJ, 890, 117
D'Onghia E., Vogelsberger M., Faucher-Giguere C.-A., Hernquist L., 2010, ApJ, 725, 353
D'Onghia E., Vogelsberger M., Hernquist L., 2013, ApJ, 766, 34
D'Onghia E., Madau P., Vera-Ciro C., Quillen A., Hernquist L., 2016, ApJ, 823, 4
Deason A. J., Belokurov V., Koposov S. E., 2018, MNRAS, 473, 2428
Debattista V. P., Sellwood J. A., 1999, ApJ, 513, L107
Debattista V. P., Gonzalez O. A., Sanderson R. E., El-Badry K., Garrison-Kimmel S., Wetzel A., Faucher-Giguère C.-A., Hopkins P. F., 2019, MNRAS, 485, 5073
Dubinski J., Kuijken K., 1995, ApJ, 442, 492
Font A. S., Navarro J. F., Stadel J., Quinn T., 2001, ApJ, 563, L1
Friske J. K. S., Schönrich R., 2019, MNRAS, 490, 5414
Gaia Collaboration et al., 2018a, A&A, 616, A1
Gaia Collaboration et al., 2018b, A&A, 616, A11
Garavito-Camargo N., Besla G., Laporte C. F. P., Johnston K. V., Gómez F. A., Watkins L. L., 2019, ApJ, 884, 51
Gauthier J.-R., Dubinski J., Widrow L. M., 2006, ApJ, 653, 1180
Giammaria M., Spagna A., Lattanzi M. G., Murante G., Re Fiorentin P., Valentini M., 2021, MNRAS, 502, 2251
Gibbons S. L. J., Belokurov V., Evans N. W., 2017, MNRAS, 464, 794
Gómez F. A., Minchev I., O'Shea B. W., Beers T. C., Bullock J. S., Purcell C. W., 2013, MNRAS, 429, 159
Gómez F. A., White S. D. M., Marinacci F., Slater C. T., Grand R. J. J., Springel V., Pakmor R., 2016, MNRAS, 456, 2779
Gómez F. A., White S. D. M., Grand R. J. J., Marinacci F., Springel V., Pakmor R., 2017, MNRAS, 465, 3446
Grady J., Belokurov V., Evans N. W., 2020, MNRAS, 492, 3128
Grillmair C. J., 2006, ApJ, 651, L29
Grion Filho D., Johnston K. V., Poggio E., Laporte C. F. P., Drimmel R., D'Onghia E., 2020, arXiv e-prints, p. arXiv:2012.07778
Haines T., D'Onghia E., Famaey B., Laporte C., Hernquist L., 2019, ApJ, 879, L15
Hayes C. R., et al., 2018, ApJ, 859, L8
Haywood M., Di Matteo P., Lehnert M. D., Snaith O., Khoperskov S., Gómez A., 2018, ApJ, 863, 113
Helmi A., 2020, arXiv e-prints, p. arXiv:2002.04340
Helmi A., Babusiaux C., Koppelman H. H., Massari D., Veljanoski J., Brown A. G. A., 2018, Nature, 563, 85
Hernquist L., 1990, ApJ, 356, 359
Hunt J. A. S., Stelea I. A., Johnston K. V., Gandhi S. S., Laporte C. F. P., Bedorf J., 2021, arXiv e-prints, p. arXiv:2107.06294
Ibata R. A., Razoumov A. O., 1998, A&A, 336, 130
Ibata R. A., Gilmore G., Irwin M. J., 1994, Nature, 370, 194
Johnston K. V., Law D. R., Majewski S. R., 2005, ApJ, 619, 800
Kallivayalil N., van der Marel R. P., Besla G., Anderson J., Alcock C., 2013, ApJ, 764, 161
Kazantzidis S., Zentner A. R., Kravtsov A. V., Bullock J. S., Debattista V. P., 2009, ApJ, 700, 1896
Kerr F. J., 1957, AJ, 62, 93
Khoperskov S., Di Matteo P., Gerhard O., Katz D., Haywood M., Combes F., Berczik P., Gomez A., 2019, A&A, 622, L6
Kim J. H., Peirani S., Kim S., Ann H. B., An S.-H., Yoon S.-J., 2014, ApJ, 789, 90
Laporte C. F. P., Gómez F. A., Besla G., Johnston K. V., Garavito-Camargo N., 2018a, MNRAS, 473, 1218
Laporte C. F. P., Johnston K. V., Gómez F. A., Garavito-Camargo N., Besla G., 2018b, MNRAS, 481, 286
Laporte C. F. P., Johnston K. V., Tzanidakis A., 2019a, MNRAS, 483, 1427
Laporte C. F. P., Minchev I., Johnston K. V., Gómez F. A., 2019b, MNRAS, 485, 3134
Laporte C. F. P., Belokurov V., Koposov S. E., Smith M. C., Hill V., 2020, MNRAS, 492, L61
Laporte C. F. P., Koposov S. E., Belokurov V., 2021, arXiv e-prints, p. arXiv:2103.12737
Law D. R., Majewski S. R., 2010, ApJ, 714, 229
Levine E. S., Blitz L., Heiles C., 2006, ApJ, 643, 881
Li T. S., et al., 2017, ApJ, 844, 74
Łokas E. L., 2019, A&A, 629, A52
López-Corredoira M., Betancort-Rijo J., Beckman J. E., 2002, A&A, 386, 169
López-Corredoira M., Garzón F., Wang H. F., Sylos Labini F., Nagy R., Chrobáková Ž., Chang J., Villarroel B., 2020, A&A, 634, A66
Masset F., Tagger M., 1997, A&A, 322, 442
McMillan P. J., 2011, MNRAS, 414, 2446
Meza A., Navarro J. F., Abadi M. G., Steinmetz M., 2005, MNRAS, 359, 93
Momany Y., Zaggia S., Gilmore G., Piotto G., Carraro G., Bedin L. R., de Angeli F., 2006, A&A, 451, 515
Navarro J. F., Abadi M. G., Venn K. A., Freeman K. C., Anguiano B., 2011, MNRAS, 412, 1203
Nelson R. W., Tremaine S., 1995, MNRAS, 275, 897
Ness M., et al., 2013, MNRAS, 430, 836
Newberg H. J., et al., 2002, ApJ, 569, 245
Peñarrubia J., Belokurov V., Evans N. W., Martínez-Delgado D., Gilmore G., Irwin M., Niederste-Ostholt M., Zucker D. B., 2010, MNRAS, 408, L26
Poggio E., et al., 2018, MNRAS, 481, L21
Poggio E., Drimmel R., Andrae R., Bailer-Jones C. A. L., Fouesneau M., Lattanzi M. G., Smart R. L., Spagna A., 2020, Nature Astronomy, 4, 590
Power C., Navarro J. F., Jenkins A., Frenk C. S., White S. D. M., Springel V., Stadel J., Quinn T., 2003, MNRAS, 338, 14
Price-Whelan A. M., Johnston K. V., Sheffield A. A., Laporte C. F. P., Sesar B., 2015, MNRAS, 452, 676
Purcell C. W., Bullock J. S., Tollerud E. J., Rocha M., Chakrabarti S., 2011, Nature, 477, 301
Quillen A. C., Dougherty J., Bagley M. B., Minchev I., Comparetta J., 2011, MNRAS, 417, 762
Ramos P., Antoja T., Figueras F., 2018, A&A, 619, A72
Recio-Blanco A., 2018, A&A, 620, A194
Reshetnikov V., Combes F., 1998, A&A, 337, 9
Rocha-Pinto H. J., Majewski S. R., Skrutskie M. F., Crane J. D., Patterson R. J., 2004, ApJ, 615, 732
Romero-Gómez M., Mateu C., Aguilar L., Figueras F., Castro-Ginard A., 2019, A&A, 627, A150
Ruiz-Lara T., Gallart C., Bernard E. J., Cassisi S., 2020, Nature Astronomy,
Sanders J. L., Binney J., 2015, MNRAS, 447, 2479
Sanders J. L., Binney J., 2016, MNRAS, 457, 2107
Schönrich R., Dehnen W., 2018, MNRAS, 478, 3809
Sellwood J. A., Athanassoula E., 1986, MNRAS, 221, 195
Sellwood J. A., Gerhard O., 2020, MNRAS, 495, 3175
Semczuk M., Łokas E. L., D'Onghia E., Athanassoula E., Debattista V. P., Hernquist L., 2020, MNRAS, 498, 3535
Sheffield A. A., Price-Whelan A. M., Tzanidakis A., Johnston K. V., Laporte C. F. P., Sesar B., 2018, ApJ, 854, 47
Shen J., Sellwood J. A., 2006, MNRAS, 370, 2
Skowron D. M., et al., 2019, Science, 365, 478
Slater C. T., et al., 2014, ApJ, 791, 9
Sparke L. S., Casertano S., 1988, MNRAS, 234, 873
Springel V., et al., 2008, MNRAS, 391, 1685
Toomre A., Toomre J., 1972, ApJ, 178, 623
Toth G., Ostriker J. P., 1992, ApJ, 389, 5
Vasiliev E., 2018, AGAMA: Action-based galaxy modeling framework (ascl:1805.008)

Vasiliev E., 2019, MNRAS, 482, 1525
Velazquez H., White S. D. M., 1999, MNRAS, 304, 254
Weinberg M. D., 1998, MNRAS, 299, 499
Weinberg M. D., Blitz L., 2006, ApJ, 641, L33
Widrow L. M., Gardner S., Yanny B., Dodelson S., Chen H.-Y., 2012, ApJ, 750, L41
Widrow L. M., Barber J., Chequers M. H., Cheng E., 2014, MNRAS, 440, 1971
Williams M. E. K., et al., 2013, MNRAS, 436, 101
Wylie S. M., Gerhard O. E., Ness M. K., Clarke J. P., Freeman K. C., Bland-Hawthorn J., 2021, arXiv e-prints, p. arXiv:2106.14298
Xu Y., Newberg H. J., Carlin J. L., Liu C., Deng L., Li J., Schönrich R., Yanny B., 2015, ApJ, 801, 105
Younger J. D., Besla G., Cox T. J., Hernquist L., Robertson B., Willman B., 2008, ApJ, 676, L21
Yurin D., Springel V., 2014, MNRAS, 444, 62
Zoccali M., et al., 2017, A&A, 599, A12
de Boer T. J. L., Belokurov V., Koposov S. E., 2018, MNRAS, 473, 647

APPENDIX A: VISUALIZING THE FOURIER DECOMPOSITION

In this Section, we give further details on the Fourier decomposition performed in Section 4. As discussed in the text, in this paper we mainly focus on the Fourier vertical terms m=0, m=1, m=2 for practical reasons. Those terms are found to be the most relevant ones (see main text), and their combination is expected to reproduce, to a first approximation, the vertical structure of the Galactic disc. Indeed, Figure A1 shows that the main features observed in the simulation (first column) are already approximated in an acceptable way by the crude sum of the first three terms (second column), although the approximation is obviously more accurate when higher order terms are included (third column). In this paper, higher order terms are not investigated for practical reasons, and we leave their exploration to future works.

To complement Figure 3, which was dedicated to the first interaction with Sgr, we here present Figure A2 and A3, showing, respectively, the evolution of the three first Fourier vertical terms in a quiescent phase after the first interaction (Regime 1), and after an interaction in the most perturbed regimes (Regime 2). As we can see, m=0 looks almost static in the quiescent phase (Figure A2), while manifests itself as fast, outgoing, ring-like vertical distortions close to an interaction (Figure 3 and A3). The m=1 vertical term moves in a prograde direction close to an interaction (Figure 3 and A3), but moves in a slow and retrograde fashion in quiescent phases (Figure 3), creating a tightly wound feature. After an interaction, the m=2 vertical term progressively winds up as well, although in Figure A3) features are more discontinuos, because of the direct influence of Sgr (which is in the Galactic plane (z=0) at R=11 kpc from the Galactic center at t=5.58 Gyr).

APPENDIX B: ZOOM LAST REGION

In this section, we reproduce Figures 4, 7 and 8, but zooming in the latest and more perturbed regimes (Figure B1, B2, top and bottom, respectively). This zooming-in can help us to identify features that otherwise would have been missed, due to the short dynamical time-scales of Regimes 2 and 3, as discussed in the main text.

APPENDIX C: ISOLATED RUN

In this section, we present a control simulation of the host galaxy described in Section 2 run in isolation. We follow the evolution of the disc for 4.5 Gyrs, using a time-step of 100 Myrs. This is done to distinguish which features in our N-body experiment can be attributed to the influence of Sgr on the disc from those already present in the isolated case. Indeed, shot noise in the particle distribution or non perfect equilibrium in the initial conditions can lead to the spontaneous formation and persistence of bending waves (Chequers & Widrow 2017). Figures C1 show the logarithm of the amplitude of the vertical displacement for the various Fourier terms $m = 0, 1$ and 2 in the isolated run. We note that both $m = 0$ and $m = 1$ terms are present in the in the initial conditions and continue to persist throughout the run, while the $m = 2$ term is practically absent. However, the amplitude of these fluctuations are significantly lower (by one to two orders of magnitude) compared to those excited by a perturbing satellite. It is also worth noting that the phase angle of the $m = 1$ term (shown in Figure C2) moves in a slow and retrograde direction, forming a leading spiral. This behaviour is also observed in the main simulation (i.e. the one including Sgr), but only in the so called quiescent phases, that is, where Sgr is far enough from an interaction (see Section 4.2.3).

APPENDIX D: VERTICAL SPECTROGRAMS AND RESONANCES

The vertical spectrograms in Figure 10 and 11 are constructed over a temporal baseline of 1 Gyr. Such temporal baseline has been chosen to identify different phases, i.e. quiescent or with one (or more) interaction(s) with Sgr, to highlight the differences in the behaviour of the Galactic disc. However, a temporal baseline of 1 Gyr implies a resolution of 6.28 km/s/kpc on the angular frequency (y-axis of the vertical spectrogram) (see Equation 13 in Chequers et al. (2018)), which is quite large. Figure D1 shows, as a complementary test, the vertical spectrogram over a baseline of 5 Gyrs, which implies a resolution of 1.26 km/s/kpc.

Figure D2 shows vertical resonances calculated in two different ways. Red curves are based on vertical frequencies obtained from the AGAMA package (Vasiliev 2018, 2019). The potentials for particles in each component in each snapshot are approximated using a spline interpolation of radial bins combined with fourier series (for disk components) and spherical harmonics (for spherical components). The actions and frequencies are then calculated using the Stackel fudge (Binney 2012; Sanders & Binney 2015, 2016).

Black curves show the outcome of an analytical approximation, where vertical frequencies are written as the sum of the contribution from the halo, the bulge and the disc $\nu_z = \sqrt{\nu^2_{z,\rm halo} + \nu^2_{z,\rm bulge} + \nu^2_{z,\rm disc}}$. Vertical frequencies from the halo and the bulge are calculated approximating them as Hernquist profiles, evaluating Eq. 5 of D'Onghia et al. (2016) at z=0. Following D'Onghia et al. (2013), we describe the disc density distribution as

$$\rho(R, z) = \frac{M_*}{4\pi z_0 R_s^2} \mathrm{sech}^2 \frac{\mathrm{z}}{\mathrm{z_0}} \exp(-\mathrm{R}/\mathrm{R_s})) \quad , \tag{D1}$$

where R_s is the scale length of the disc, z_0 is the scale height of the disc, and M_* is the mass of the disc. Using the above density distribution, the vertical frequency $\nu^2_{z,\rm disc}$ can be approximated as

$$\nu^2_{z,\rm disc} = \frac{GM_*}{z_0 R_s^2} \exp(-R/R_s) \quad . \tag{D2}$$

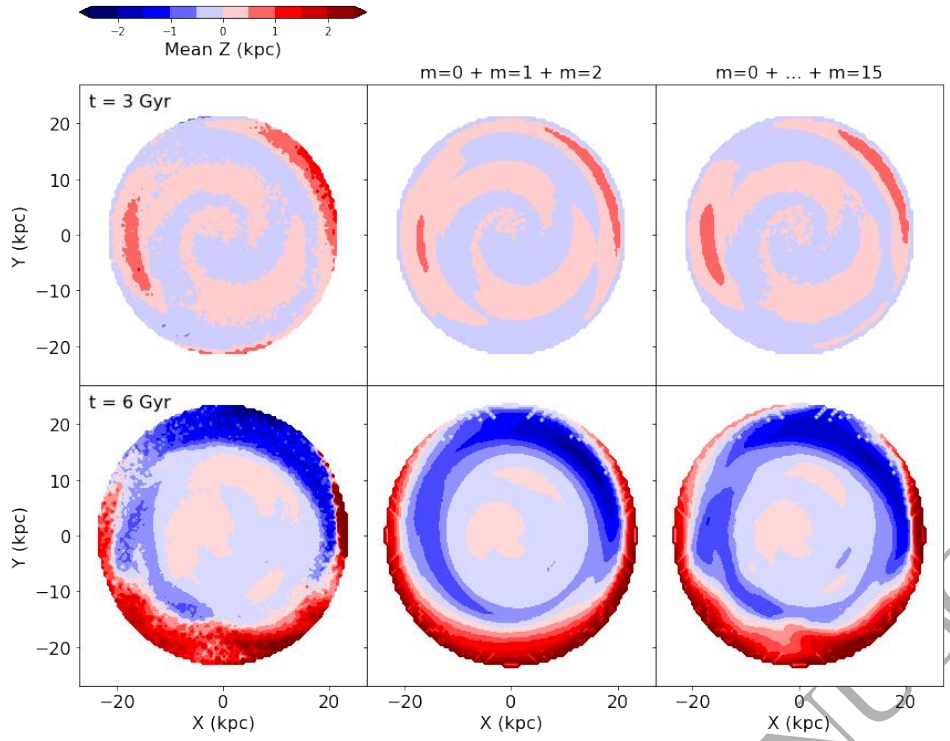

Figure A1. The mean vertical displacement of the Galactic disc (first column) compared to the corresponding Fourier decomposition, using the sum of the first three vertical terms m=0, m=1 and m=2 only (second column) and the first sixteen terms m=0, ..., m=15 (third column). Two snapshots were considered to test the validity of the approximation both in the early stages of the simulation (first column) and the more perturbed regimes (second row).

Since the analytical approximation reflects the initial conditions, the agreement between the black and red curves is better at the beginning of the simulation (upper left panel) and becomes worse at the end of the simulation (lower right panel).

This paper has been typeset from a TEX/LATEX file prepared by the author.

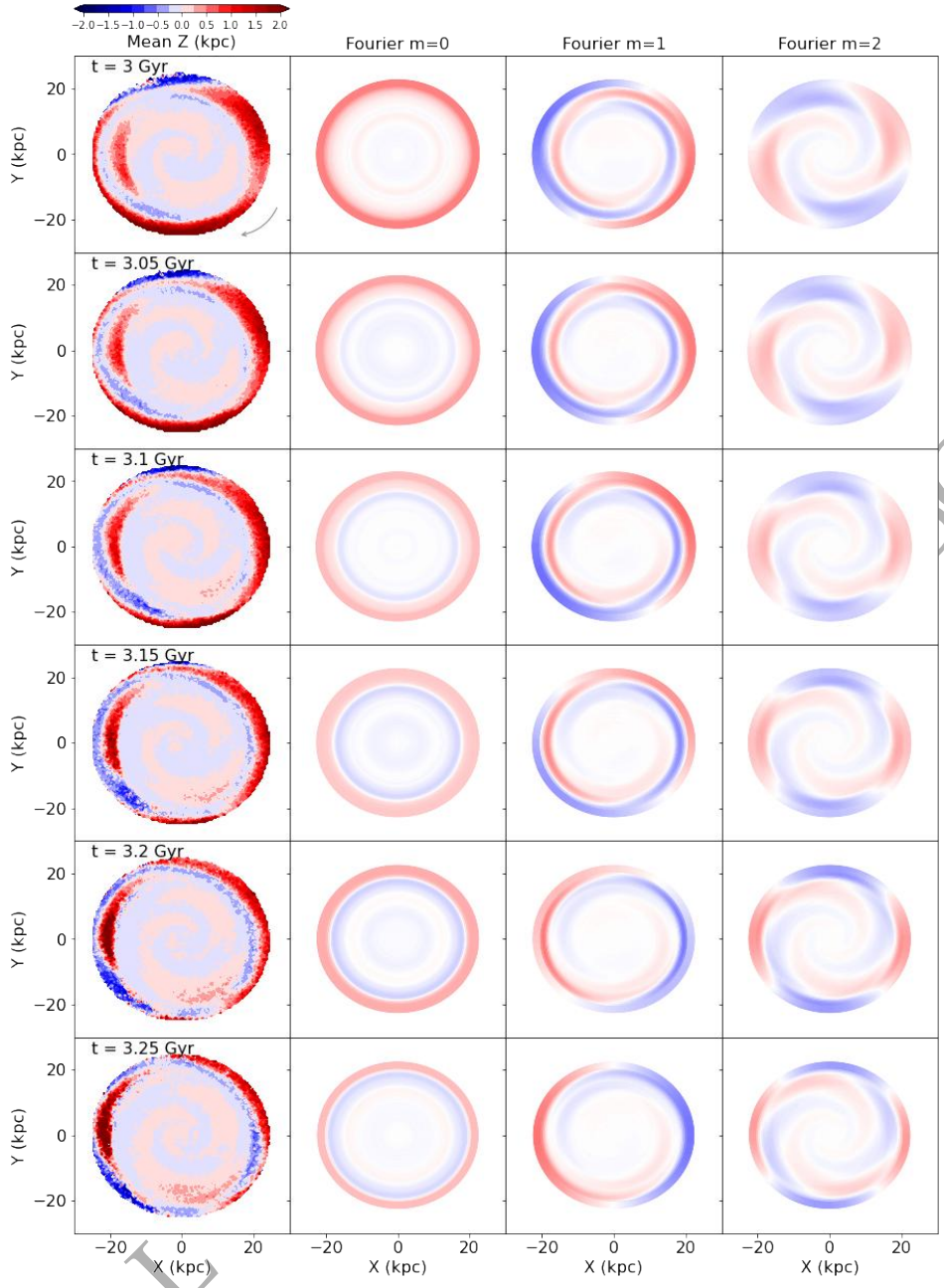

Figure A2. Same as Figure 3, but considering a quiescent phase in Regime 1.

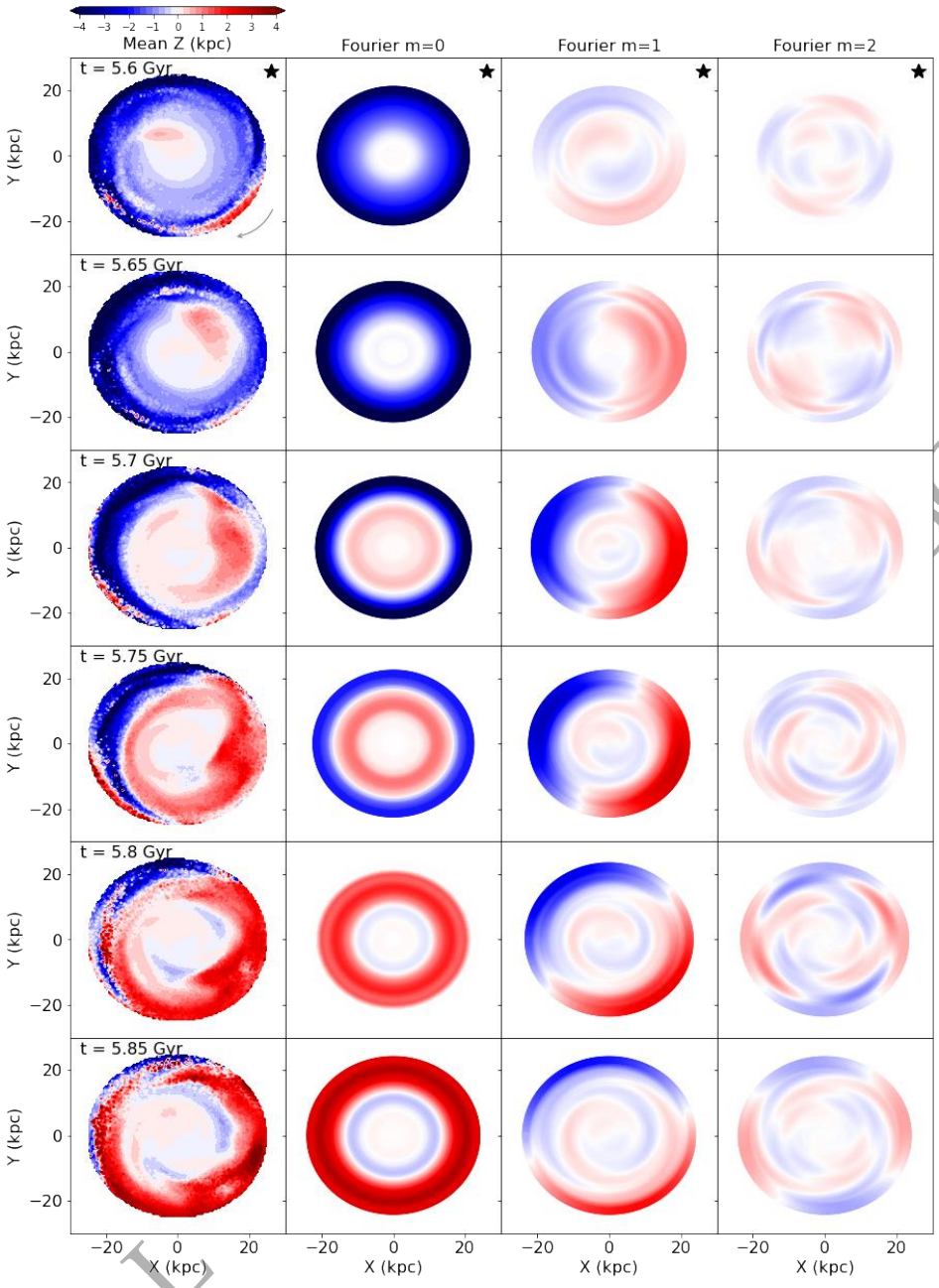

Figure A3. Same as Figure 3, but considering Regime 2.

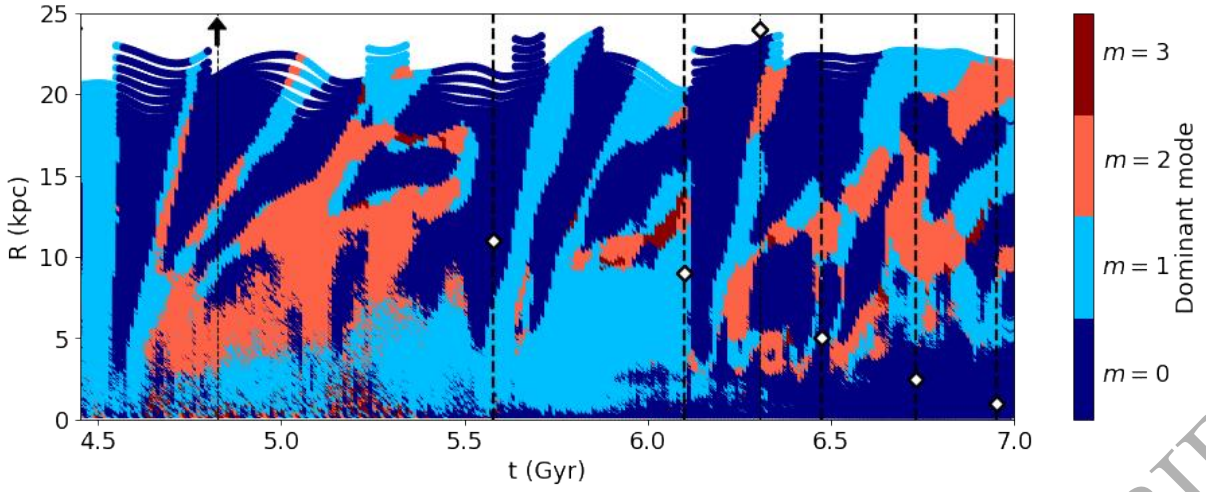

Figure B1. Same as Figure 4 , but zooming in the most perturbed region.

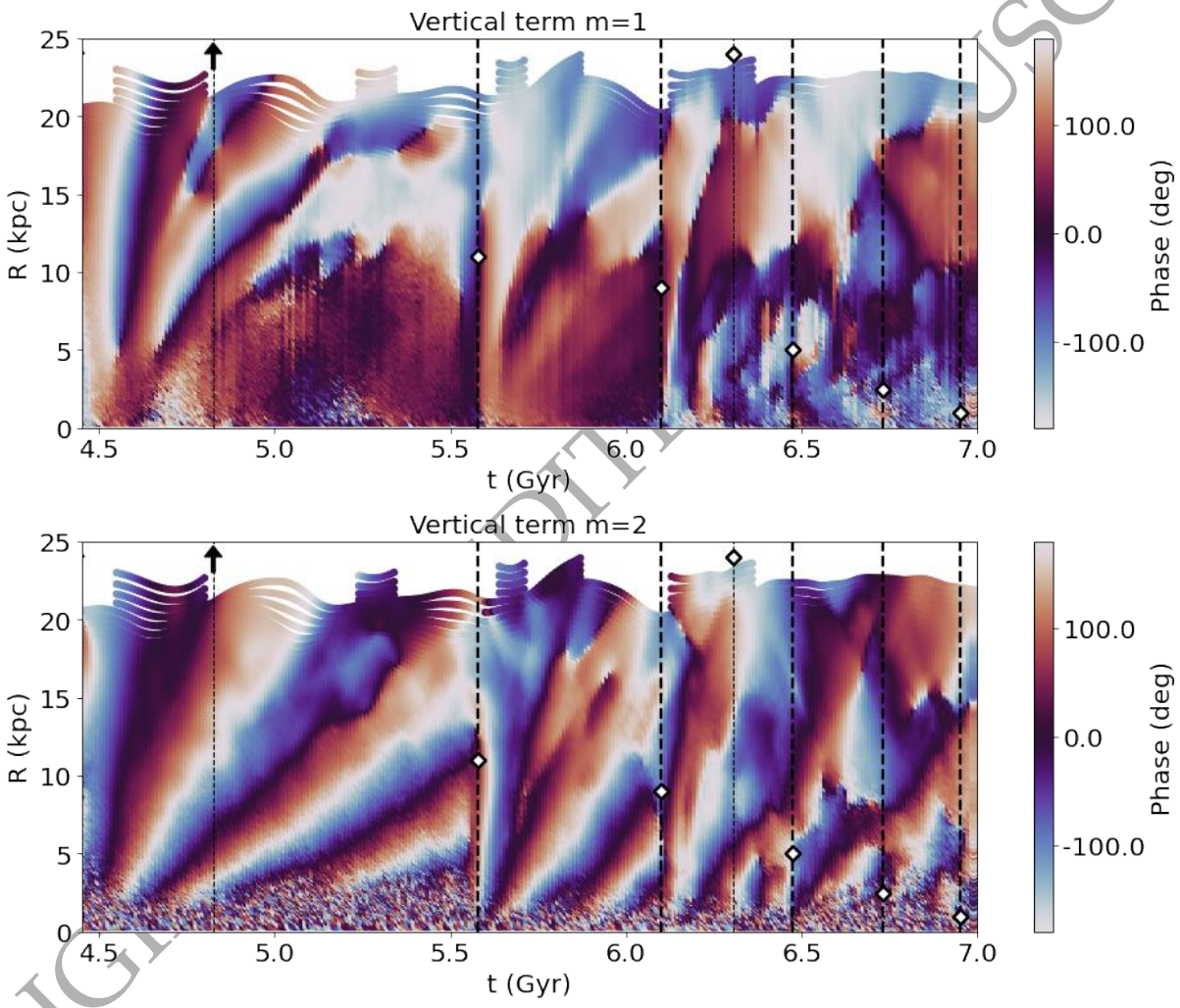

Figure B2. Same as Figure 7 (top) and Figure 8 (bottom), but zooming in the most perturbed region.

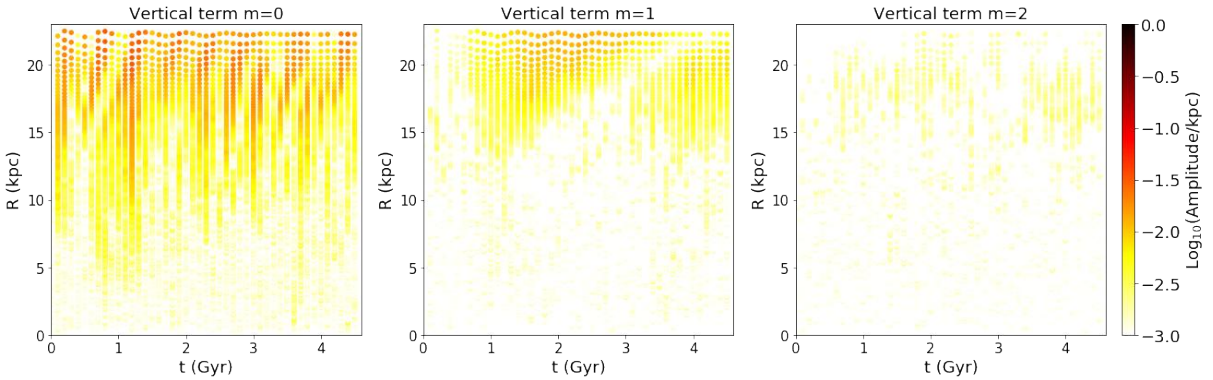

Figure C1. Amplitude of the $m = 0$ (left panel), $m = 1$ (middle panel) and $m = 2$ vertical terms in the isolated run.

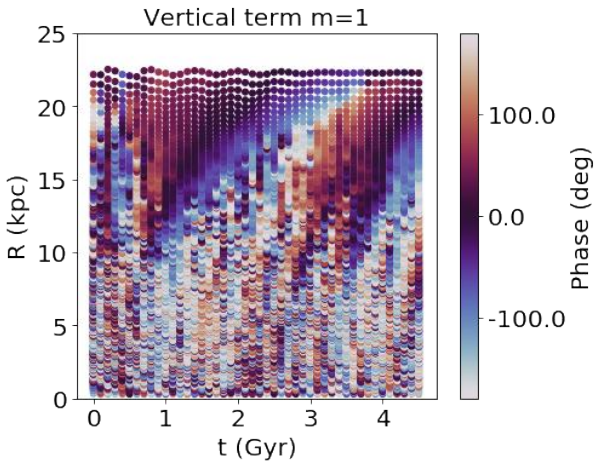

Figure C2. Phase angle of the $m = 1$ vertical term in the isolated run.

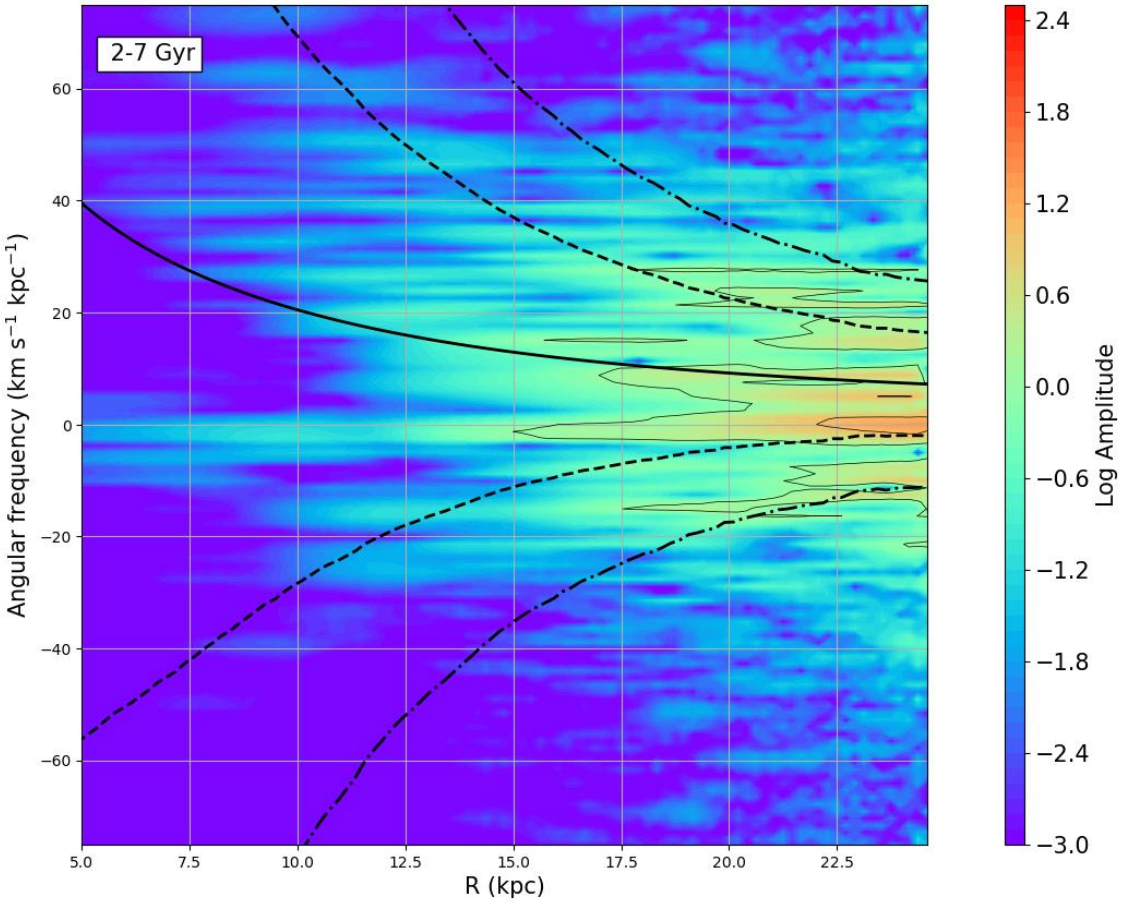

Figure D1. Same as Figure 10, but showing the vertical spectrogram for the m=1 term over a time baseline of 5 Gyr (from 2 and 7 Gyr in the simulation). Solid, dashed and dotted curves are as in Figure 10.

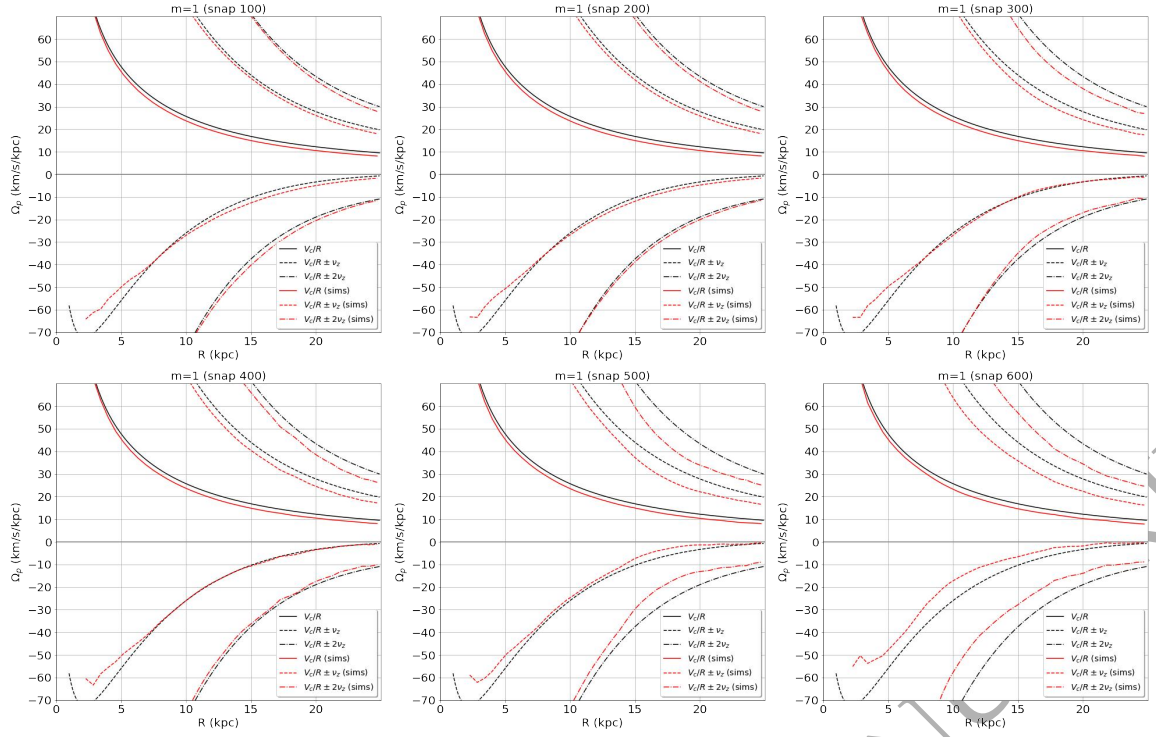

Figure D2. Comparison between vertical resonances from the analytical approximation (black curves) and those obtained using vertical frequencies from AGAMA at different times (red curves). (Top panels, from left to right: t=1,2,3 Gyr. Bottom panels, from left to right: 4,5,6 Gyr.) Solid lines show corotation, while the dashed and dashed-dotted curves show, respectively, $\Omega \pm \nu_z$ and $\Omega \pm 2\nu_z$ vertical resonances.